AD-774 894

FRAGMENTATION ANALYSIS-FUNDAMENTAL PROCESSES

L. S. Sundae, et al

Bureau of Mines
Twin Cities, Minnesota

31 December 1973

DISTRIBUTED BY:

NTIS
National Technical Information Service
U. S. DEPARTMENT OF COMMERCE
5285 Port Royal Road, Springfield Va. 22151

UNCLASSIFIED

SECURITY CLASSIFICATION OF THIS PAGE (When Data Entered)

AD-774 894

REPORT DOCUMENTATION PAGE

READ INSTRUCTIONS BEFORE COMPLETING FORM

1. REPORT NUMBER P10-4	2. GOVT ACCESSION NO.	3. RECIPIENT'S CATALOG NUMBER
4. TITLE (and Subtitle) Fragmentation Analysis - Fundamental Processes		5. TYPE OF REPORT & PERIOD COVERED Technical Report Final Jan.'72 - Dec.'73
		6. PERFORMING ORG. REPORT NUMBER
7. AUTHOR(s) L. S. Sundae, D. I. Kurth, and C. W. Schultz		8. CONTRACT OR GRANT NUMBER(s)
9. PERFORMING ORGANIZATION NAME AND ADDRESS U.S. Bureau of Mines Twin Cities Mining Research Center P.O. Box 1660 Twin Cities, Minnesota 55111		10. PROGRAM ELEMENT, PROJECT, TASK AREA & WORK UNIT NUMBERS Program element 62701D ARPA Order 1579 AM3 2B32/F53106
11. CONTROLLING OFFICE NAME AND ADDRESS Advanced Research Projects Agency 1400 Wilson Boulevard Arlington, Virginia 22209		12. REPORT DATE Dec. 31, 1973
		13. NUMBER OF PAGES ~~90~~ 98
14. MONITORING AGENCY NAME & ADDRESS(if different from Controlling Office) U.S. Bureau of Mines Twin Cities Mining Research Center P.O. Box 1660 Twin Cities, Minnesota 55111		15. SECURITY CLASS. (of this report) Unclassified
		15a. DECLASSIFICATION/DOWNGRADING SCHEDULE

16. DISTRIBUTION STATEMENT (of this Report)

Distribution of this document is unlimited.

17. DISTRIBUTION STATEMENT (of the abstract entered in Block 20, if different from Report)

18. SUPPLEMENTARY NOTES

19. KEY WORDS (Continue on reverse side if necessary and identify by block number)

Rock Fragmentation
Product Size Distribution
Energy Input
Rock Fabric Analysis
Comminution

20. ABSTRACT (Continue on reverse side if necessary and identify by block number)

To investigate the effect of energy on rock fragmentation, initial testing was carried out using a drop test device. A total of 180 specimens of Wausau quartzite and anorthosite of 3.0 to 3.5 inch size were fragmented in this device. Analysis of energy limitations of this device and other test results led to the conclusion that a device supplying higher energy should also be used. Consequently, an impact pendulum test device was designed and constructed.

DD FORM 1 JAN 73 1473 EDITION OF 1 NOV 65 IS OBSOLETE

UNCLASSIFIED

SECURITY CLASSIFICATION OF THIS PAGE (When Data Entered)

AD-774894

20. ABSTRACT (Continued)

An analysis of the fragment distribution results of the drop tests showed that the energy applied was approximately inversely proportional to the mean fragment size. However, these results were not totally conclusive because of the limited energy available and the narrow band of drop heights available.

A total of 270 irregular 3.0 to 3.5 inch specimens and 150 disc-shaped specimens of Wausau quartzite, anorthosite, and Felch marble were then fragmented with the impact pendulum device. This device was instrumented so as to provide data for calculating the specific crushing energy that went into each fragmentation event. Computer programs were written to analyze sieve data and to provide energy calculations. Results indicated that a power law could be obtained that provided the inverse relation between specific crushing energy and mean fragment size.

Form Approved
Budget Bureau No.: 22-R0293

Final Technical Report

ARPA Order No.: 1579 Amendment 3

Effective Date: Jan. 1, 1972

Program Code: 2F10

Expiration Date: Dec. 31, 1973

Originating Agency: U.S. Bureau of Mines
Twin Cities Mining
Research Center
P.O. Box 1660
Twin Cities, Minn.
55111

Amount Funded $33,000

Principal Investigator: Donald I. Kurth
Telephone No.: 612/725-4549

Title: Fragmentation Analysis - Fundamental Processes

Sponsored by:

Advanced Research Projects Agency
1400 Wilson Boulevard
Arlington, Virginia 22209

ib

FINAL TECHNICAL REPORT

Bureau of Mines In-house Research

Fragmentation Analysis - Fundamental Processes

Prepared by L. S. Sundae, D. I. Kurth, and C. W. Schultz

Sponsored by
Advanced Research Projects Agency
ARPA Order No. 1579, Amendment No. 3
Program Code No. 2F10

CONTENTS

ILLUSTRATIONS

ILLUSTRATIONS (Continued)

TABLES

TABLES (Continued)

TABLES (Continued)

FRAGMENTATION ANALYSIS - FUNDAMENTAL PROCESSES

INTRODUCTION

In the study of rock fragmentation there are two fundamental problem areas which can be investigated. These are (1) investigation of the conditions under which fragmentation occurs and (2) investigation of the results of fragmenting processes.

The first of these problem areas is where the greatest effort has been and is being expended. Most of this work, however, should be categorized as studies of rock failure and/or fracture rather than rock fragmentation. The significance of rock fragmentation is emphasized by various efforts to relate failure mechanisms to the strength of rock.

The second problem area is justifiable from an operational viewpoint. Rock excavation involves fragmentation processes, such as drilling, blasting, and mechanical excavation. Thus, because the nature of the product of a fragmentation process is a function of the process itself, and in turn influences the selection of subsequent processes such as further fragmenting, handling, and transporting the rock, it is important that the nature of fragmentation products be known.

Intuitively, a relationship should exist between a product size distribution and the energy input from the nature of the fragmenting process and the rock properties. Unfortunately, no such relationship has been defined. This then was the purpose of this investigation.

Specifically, the objective of this investigation was to determine the relationship between energy input and the size distribution resulting from a single elementary fragmenting event. The actual investigation was conducted primarily to obtain the value of the parameters that define the strength of the material and the process and to relate the strength parameters with the mechanical properties of the material.

ACKNOWLEDGMENTS

The authors are greatly indebted to Walter G. Krawza and Richard L. Fischer for their help in equipment calibration by using high-speed photography; Sathit Tandanand, A. Aly Selim, and Bruce D. Hanson for valuable suggestions in data analysis; V. W. Dellorfano and his staff in equipment fabrication and instrumentation; and Orin M. Peterson for his help in data analysis.

TECHNICAL REPORT SUMMARY

The main results of this project were as follows: (1) The size distributions of rock fragments resulting from a single elementary fragmentation event (comminution of a given size rock) was obtained. (2) This distribution data was used to determine the elements of the breakage matrix, which relates the input size distribution to the output size distribution. (3) A power law relationship between specific crushing energy (or input energy) and product size was developed.

Three types of rocks were tested in two types of comminution events--drop tests and impact pendulum tests. The series of drop tests were considered to be preliminary tests to the main series of impact pendulum tests. The purpose of these drop tests were twofold--to provide an alternate source of comminution and to evaluate any possible effect of loading rate on breakage. The loading rate had no apparent effect. Composite normal distributions were used to fit the fragment distribution data from the drop tests.

The impact pendulum tests were of the most interest. It was found possible to measure to a reasonable accuracy the velocities of the moving parts before and after impact so that specific crushing energy could be calculated. A number of different distributions were fitted to the sieve data (resultant fragment distributions) and it was found that the normal distribution provided the best fit.

From the distribution data, the breakage, matrix, which has elements expressing the probabilities of decreasing from one size fragment to a smaller one, was determined. The relationship of input (feed) distribution to output (product) distribution was found, under certain assumptions, to be given by $\vec{p} = B' \vec{f}$, where $\vec{p}$ is the product vector, B' is the simplified breakage matrix and $\vec{f}$ is the feed vector.

Relationships between specific crushing energy and average fragment size were developed for the impact pendulum tests. For the three rock types tested, one such relationship was a power law function of the form

$$E/V_o = a/\mu^b,$$

where

E/V_o = specific crushing energy,

a,b = constants related to the breakage process and the rock type,

and μ = average fragment size.

An alternate relationship between specific crushing energy and average fragment size is the Charles' law formulation.

$$E/V_o = K\,[1/\chi_2^{\,n-1} - 1/\chi_1^{\,n-1}],$$

where

E/V_o = specific crushing energy,

K,n = constants related to the breakage process and the rock type,

χ_1 = initial specimen sieve size,

and χ_2 = average product sieve size.

Values of a,b and K,n were determined from experimental data on irregular and disc specimens of Wausau quartzite, anorthosite, and Felch marble.

EXPERIMENTAL PROGRAM

Plan of Work

To simulate a single event fragmentation process that is similar to a real fragmentation process such as occurs with a crusher, it was decided to use random-shaped specimens having a single given initial sieve size. Disc-shaped specimens that were relatively defect-free were also used for greater homogeneity of breakage with fewer specimens. Also the breakage results of the disc-shaped specimens could be compared with the breakage results of the random-shaped specimens. This comparison was essential because it shows the two extremes of brittle fracture (see also (11)).

A preliminary experiment (see DATA ANALYSIS section) was designed to determine the total number of tests required to achieve average values representative of sample populations. Another test series (see DATA ANALYSIS section) was designed to study the effect of specimen size and shape for the size range tested in this test program.

Drop test equipment was initially used to provide some of the data necessary to achieve the objectives of this test program. It was known that the drop test data would not account for the energy dissipated into the impact plate, the kinetic energy utilized in scattering broken fragments, heat, or acoustic energy. Therefore a low velocity impact pendulum was later designed to improve on the drop tests.

For the impact pendulum tests, (see DATA ANALYSIS section) most of the excessive energy available is utilized by the moving parts of the test apparatus and is accounted for by (1) determining the velocity of the impact pendulum, first piston, specimen, second piston, and second pendulum, and (2) accounting for heat, vibration, acoustic, and friction energy by a calibration (no specimen) test procedure.

Drop Test Apparatus

A drop test apparatus was fabricated and installed as shown in figure 1. To minimize secondary breakage (multiple comminution of some fragments), the inside of this chamber was lined with foam and polyethylene sheet. The specimen was placed on top of trap doors in a platform and hoisted to the desired height. As soon as the platform reached a specified height, the specimen was discharged by a mechanical release pin attached to the trapdoor. Three drop heights of 25, 30, and 35 ft were selected to provide impact velocities of 40.1, 43.9, and 47.4 ft/sec and impact energies of approximately 62.5, 75.0, and 87.5 ft-lb for a typical 2.5 lb specimen. The broken material was retained in a wooden impact chamber and later was swept, bagged, labelled, and sieved manually.

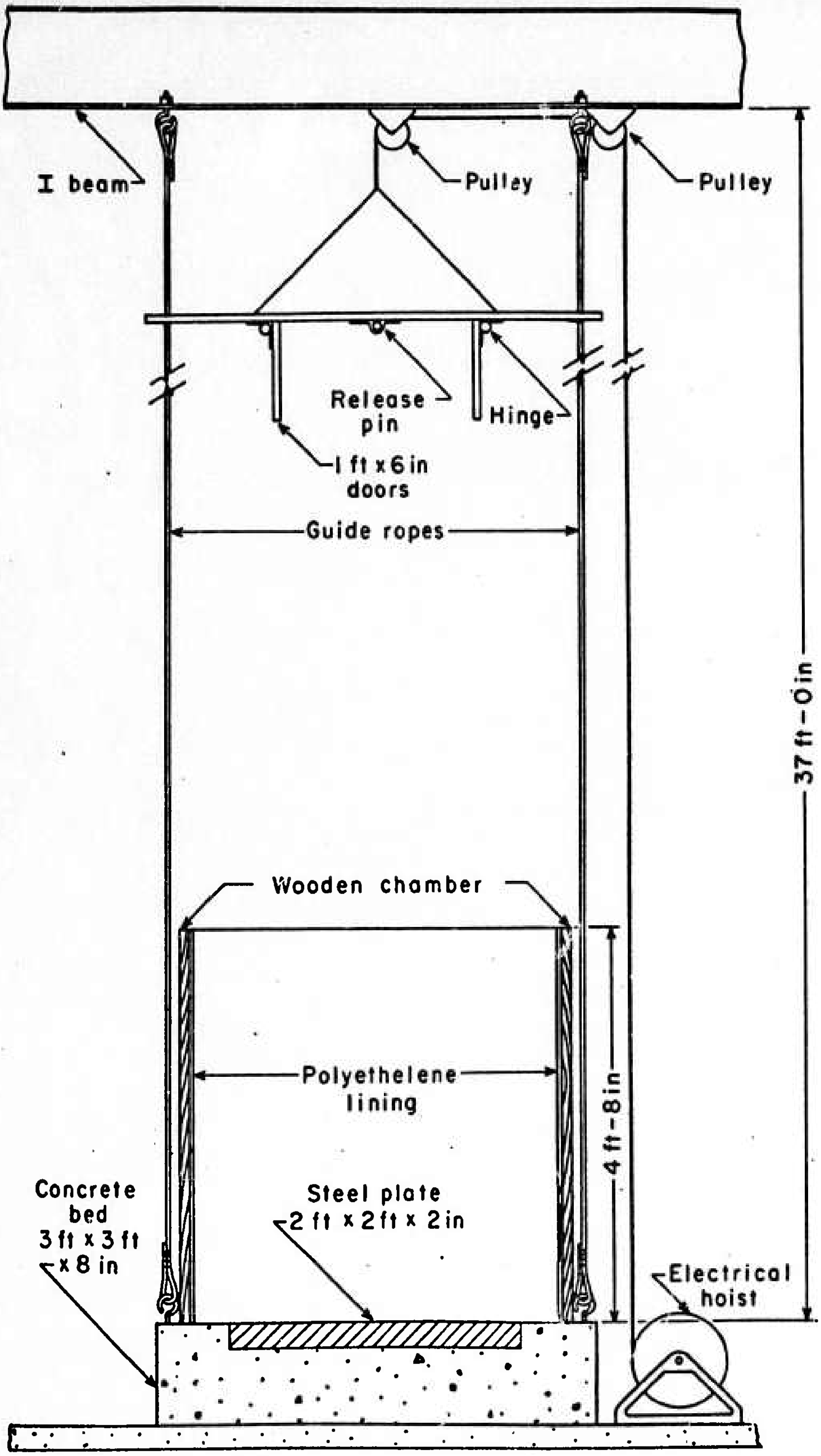

Figure 1. Drop test apparatus.

One hundred and eighty specimens (ninety of Wausau quartzite and ninety of anorthosite) were then fragmented in the major test series for these drop tests. Thirty specimens of each rock type were dropped from heights of 25, 30, and 35 ft. The fragments from each specimen were then sieved to determine composite size distribution of fragments in each sieve class.

Impact Pendulum Test Apparatus

A low velocity impact pendulum (Fig. 2) was constructed to provide higher energy for rock fragmentation and to investigate the effect of varying input energy on size distribution of broken material. It mainly consisted of an impact pendulum (162.5 lb), first piston (38.9 lb), second piston (41.5 lb), and second pendulum (269.0 lb). The pistons were supported on two sets of roller bearings. The parts of the pistons were enclosed in the impact chamber. The test specimens were suspended by a string from the ceiling of this chamber to rest between two piston heads (platens).

The test procedure consisted of (1) placing a specimen enclosed in a plastic bag between the platens (the bag overlaps the platens), (2) releasing the impact pendulum, (3) recording the horizontal distance the rebound pendulum has travelled, (4) arresting the motion of both pendulums after impact and travel measurement have taken place, (5) recording the timer reading.

Test Specimens

Rocks of potential use in the present investigation may be such that their constituents and properties vary considerably from one specimen to another. To minimize such variations, three monomineralic rocks - Wausau quartzite, anorthosite, and Felch marble were selected. The minerals that these rocks are composed of represent a large proportion of rock forming minerals found in tunneling and other excavation projects.

Irregular specimens ranging in size from 3 in to 3.5 in were acquired from muck piles of quarry blasts. The specimens which did not meet visual inspection standards for uniformity of mineral composition and absence of macroscopic flaws were rejected. Selected specimens were washed, dried, and weighed.

In order to determine the physical properties of these rocks, a block of each rock type measuring 18 by 18 by 18 in was acquired, from which 10 specimens were cut. These physical properties are presented in Table 1. Disc specimens (2 in diameter x 1 in thick) were also prepared from these blocks by cutting and coring. Again badly flawed specimens were rejected.

TABLE 1. - Physical properties of Wausau quartzite, anorthosite, and Felch marble

Property	Rock type		
	Wausau quartzite	Anorthosite	Felch marble
Compressive strength........MN/m^2	285.7	221.	172.50
..........psi	41,437.	32,053.	25,019.
Tensile strength............MN/m^2	5.12	8.97	6.78
..............psi	742.	1301.	983.
Shore hardness..................	111.6	91.7	65.1
Pulse velocity..............m/sec	5130.	6866.	6686.
.............ft/sec	16,831.	22,526.	21,936.
Bar velocity................m/sec	4679.	5,742.	5,952.
...............ft/sec	15,351.	18,839.	19,528.
Torsional velocity..........m/sec	3383.	3,396.	3,677.
.........ft/sec	11,099.	11,142.	12,064.
Static Young's modulus......MN/m^2	7.249×10^4	4.085×10^4	4.318×10^4
........psi	10.51×10^6	5.925×10^6	6.263×10^6
Dynamic Young's modulus*....MN/m^2	5.74×10^4	8.971×10^4	10.35×10^4
......psi	8.33×10^6	13.01×10^6	15.01×10^6
Dynamic shear modulus**.....MN/m^2	3.000×10^4	3.115×10^4	3.95×10^4
.......psi	4.351×10^6	4.518×10^6	5.73×10^6
Poisson's ratio***...............	.251	.310	.268
Density....................g/cm^3	2.649	2.699	2.899
....................lb/ft^3	165.4	168.5	181.0

* - Calculated from bar velocity
** - Calculated from torsional velocity
*** - Derived from ratio of longitudinal pulse velocity to longitudinal bar velocity

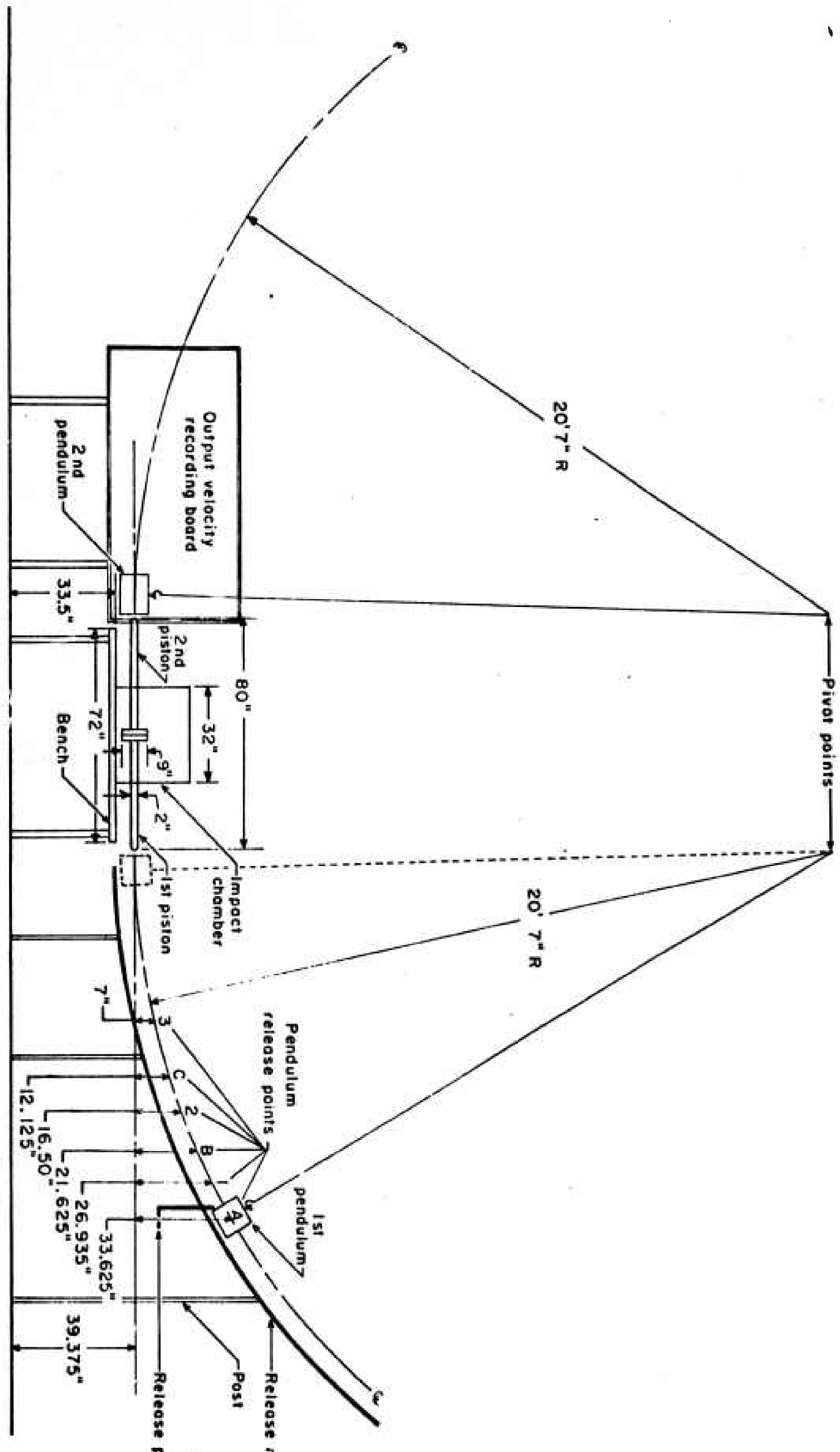

Figure 2. Impact pendulum apparatus.

Wausau quartzite is a Precambrian metamorphic rock exposed in the Rib Hill Mountains southwest of Wausau, Wisconsin, and it is commercially known as Wausau quartzite. It consists of 98.2 percent quartzite, 0.5 percent coarse amphibole, 0.4 percent fine amphibole, and 0.4 percent iron oxide, and 0.1 percent feldspar. The impurities are scattered throughout the rock at quartz grain boundaries. The quartz crystals vary in diameter from 3mm to 8mm.

Anorthosite is a monomineralic rock intrusion in the Duluth Gabbro complex nearly 5 miles north of Beaver Bay, Minn. It is coarse grained, light green in color and consists of more than 95 percent plagioclase.

Felch marble is a dolomite named for a typical development at Felch Mountain in Dickinson County, Michigan. It is mined from a vein deposit intrusion in Precambrian sandstone by underground mining. The marble is white in color, coarse in texture, and has small impurities. In addition to calcium-magnesium carbonate, it contains nearly 25 percent calcium-magnesium silicate.

Although all three rock types were metamorphic in origin, monomineralic in appearance, crystalline, and similar in texture and grain size, the shape of samples of Wausau quartzite were frequently different from the other two rock types. This rock comes in three relatively distinct shapes--flat, elongated, and equidimensional, whereas anorthosite and Felch marble were more generally equidimensional in shape. The Wausau quartzite shapes are probably related to metamorphic and tectonic activities during the cooling period of the Rib Hill mountain region.

Fabric Analysis

The mapping of both macroscopic cracks and microscopic flaws revealed that all three rock types contained a large number of cracks and flaws. The distribution was random. The cracks and flaws formed a network, one crack or flaw crossing many others. It was not found possible to determine the number or size of cracks in any individual specimen. Figure 3 illustrates problems associated with crack density or crack propagation theories of rock fragmentation. This photograph is typical of rock specimens used in this investigation. Macroscopic cracks are few in number and very little is known about their definite origin, while microscopic flaws are numerous and probably associated with grain boundaries.

It seems obvious from this photograph that the effects of macroscopic cracks are more significant than the effects of microscopic flaws on certain rock properties. This is only a qualitative conjecture because it is not possible to verify or quantify this statement with experimental evidence. In certain cases, macroscopic cracks are quite thin and their direction is irregular due to joining or intersection of other cracks. If there are microscopic flaws beneath the surface, their effect is unknown. The direction of the crack propagation is not related to the direction of the load. Also, it is not possible to determine the true surface area of an irregular fracture path. Thus it was concluded that it was not feasible to determine the quantitative effect of macroscopic cracks or microscopic flaws in this rock fragmentation project or to include such an effect in the experimental design.

BACKGROUND

Fragment Distributions

A number of both empirical and theoretical equations have been used to describe the size distribution of broken material. A brief account of the major equations is given below. The data is usually expressed as the cumulative fraction or cumulative percentage by weight under size, Y, (or over size 1 - Y = Y') in relation to size x.

Three of the common equations used are as follows:

(1) Gates - Gaudin - Schuhmann (8, 6, 15):

$$Y = \left(\frac{x}{k}\right)^m \tag{1}$$

where Y = cumulative fraction finer than size x,
m = distribution modulus referring to the spread of the distribution, i.e., to the slope of the line on log-log paper,
k = size modulus[2/].

[2/] Schuhmann (15) expressed the size distribution of broken material by defining an extrapolated intercept from the linear part (fines) of the cumulative curve. The extrapolation of the linear portion of the curve to the 100 percent passing ordinate defines the 100 percent size modulus, k. This method of expressing the product size has been used by many investigators. (Similarly, an 80 percent modulus defined as the same line extrapolated to the 80 percent passing ordinate has also been used.)

---

(2) Rosin - Rammler (14):

$$Y = 1 - \exp(bx^n) \tag{2}$$

where Y = cumulative fraction finer than size x,
b and n are similar to the constants m and $1/k^m$ in equation 1,

(3) Gaudin - Meloy (7):

$$Y = 1 - \left(1 - \frac{x}{x_o}\right)^{r_1} \tag{3}$$

where Y = cumulative fraction finer than size x,
x_o = 100 percent passing size, and
r_1 = parameter related to the mean spacing of the flaws.

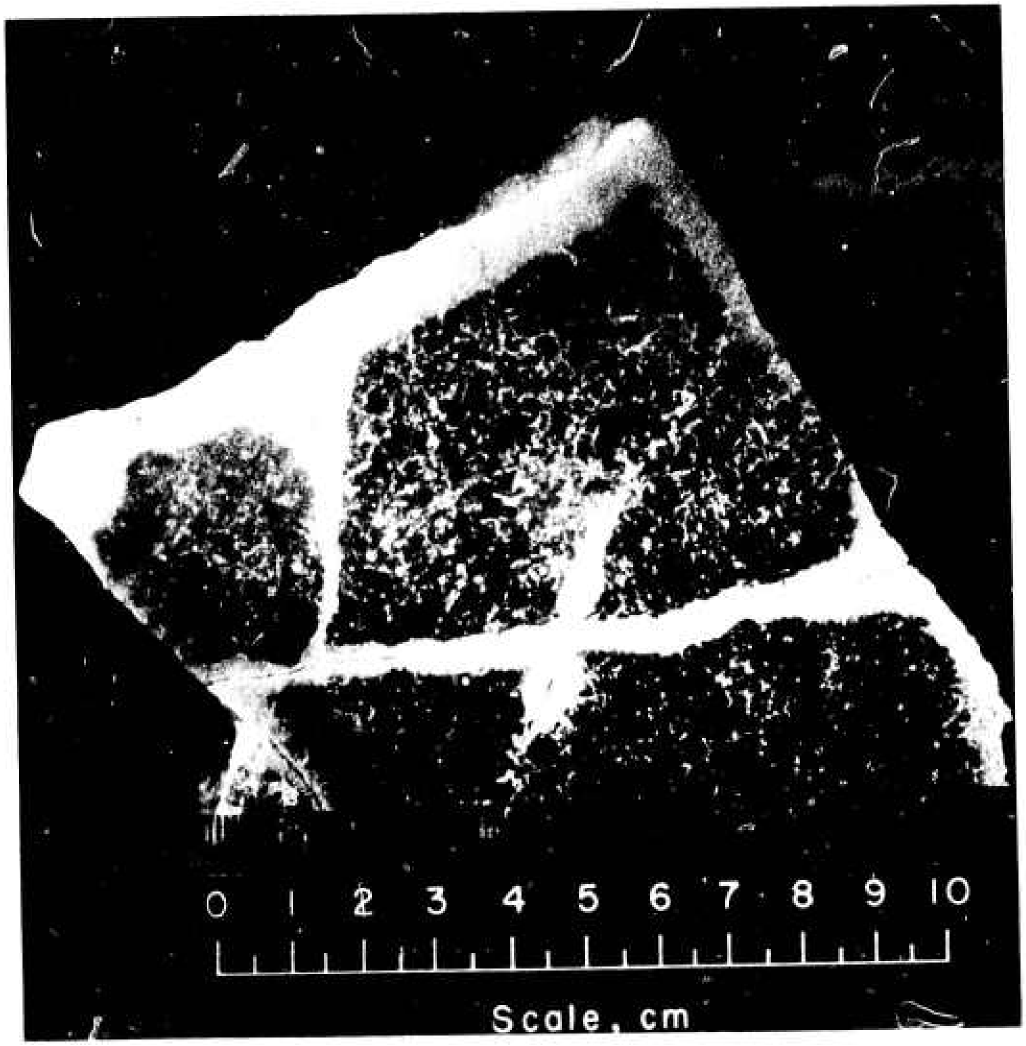

FIGURE 3. - Typical photograph of macroscopic and microscopic flaws in Wausau quartzite specimen using dye penetrant.

Gaudin and Meloy suggested that their equation describes the distribution curve in the coarse range while the Gates - Gaudin - Schumann and Rosin - Rammler equations describe the distribution curve in the fine range. Thus an overall satisfactory curve fit would require the combination of these two equations. Gaudin and Meloy derived their equation by using probability theory.

Bergstrom (1A) suggested that the equation

$$Y = [1 - (1 - \frac{x}{x_o})^{r_2}]^{q_1} \tag{4}$$

combines the fine and coarse size curve fitting capabilities of equations 1 and 2. This equation is then an extension of equation 3. Here
q_1 = constant for improved curve fit,
x_o = 100 percent passing size, and
r_2 = parameter related to the mean spacing of the flaws.

Harris (10) modified the Bergstrom equation 4 by inserting still another exponent, as follows:

$$Y = 1 - \{1 - [1 - (\frac{x}{x_o})^{s}]^{r_3}\}^{q_2} \tag{5}$$

He claimed no physical basis for the insertion of q_2 in equation 5. He merely inserted this term for the sake of increased curve fitting flexibility. It is supposedly feasible to determine the values of r_2 and q_1 or of s, r_3, and q_2 simultaneously by using graphical or computational methods. However, these constants cannot be related directly to physical properties of the material or to the type of test.

Gilvarry (9) derived the following theoretical equation

$$Y = 1 - \exp\left[-(\frac{x}{k}) - (\frac{x}{j})^2 - (\frac{x}{i})^3\right] \tag{6}$$

based on the premise that fracture is caused by stress activated flaws randomly distributed in the volume, in fracture surfaces, and in the edges produced by fracture surfaces. The parameters in equation 6 are defined as follows:

- Y = cumulative fraction finer than size x,
- x = mean linear dimension of a fragment,
- k = constant related to the mean spacing of edge flaws with respect to x,
- j = constant related to mean spacing of surface flaws with respect to x, and
- i = constant related to mean spacing of volume flaws with respect to x.

For small values of x, the higher order terms drop from this equation and it reduces to

$$Y = 1 - \exp\left[- \frac{x}{k} \right] \tag{7}$$

This expression is equivalent to the Rosin-Rammler equation (2) for n = 1.

When x becomes small in equation 7, the dominant term of the series expansion of the exponential becomes 1 so that

$$Y = \frac{x}{k} . \tag{8}$$

This result is the same as equation 1 for the case m = 1.

Klimpell and Austin (12) verified equations 1-3 by using statistical theory to describe the fragment sizes obtained in simple fracture of brittle solids producing large particles.

Epstein (5) constructed a statistical model for the breakage mechanism and the breakage process based on the theory of probability. He found that under certain conditions it can be proved that the distribution of broken material is asymptotically log-normal.

From the literature cited above, it was concluded that the majority of investigators have used various forms or limiting cases of the following functions:

The exponential distribution--

$$Y = 1 - \exp(-\lambda x), \tag{9}$$

the two parameter Weibull distribution--

$$Y = 1 - \exp(-x/\sigma)^{\alpha}, \tag{10}$$

the log-normal distribution--

$$Y \simeq \int_{o}^{x} (1/B\, x\sqrt{2\pi}) \exp\left[- (\log x - \log \alpha_1)^2/2B^2\right] dx, \text{ and} \tag{11}$$

the power function--

$$Y = ax^{b} \tag{12}$$

where Y is the cumulative fraction finer than size x, and where λ; α,σ; α_1,B; a,b are parameters of the four functions respectively.

Two other distributions used in statistics were added to the list of the above four functions. These are as follows:

the two parameter log-Weibull distribution--

$$Y = 1 - \exp \{-(\exp x)/\theta)^{\beta}\}, \tag{13}$$

and the normal distribution--

$$Y = \int_0^x (1/\sigma \sqrt{2\pi}) \exp \{-(x - \mu_1)^2/2\sigma^2\} dx \tag{14}$$

where β, θ; μ_1, σ are parameters of the two functions respectively.

It was not feasible to select any single equation from equations 9-14 which describes all the size distributions of broken material that were found in this investigation. For this reason, it was decided to use a linear regression computer program incorporating the six equations 9-14 and to determine the coefficients of correlation in all six cases (see DATA ANALYSIS section).

For primary breakage, the cumulative percentage of weight retained (or passing) plotted against sieve size opening on a log-log grid or log normal grid or on other special grids frequently gives a straight line over a large section of the plot. In the majority of cases the overall curve consists of a line with a slope in the fine range which is different from and usually less than unity, while in the coarse range there is a curve or another line with a slope usually higher than unity. In other words, the distribution plot can be separated into the plots of two distributions represented by two separate equations, one for the fine range and another for the coarse range.

There is no evidence to support the hypothesis that the same fracture patterns exist throughout all size ranges. There is also no evidence to support the hypothesis that the change in fracture pattern is exclusively related to a change in the slope of the distribution curve. Irregularities encountered in the slope may be related to such things as plastic deformation at contact points (where high stress concentration occurs), test method, specimen geometry, and secondary breakage.

Energy Relationships in Fragmentation

As mentioned in the Fragment Distributions section, the straight line representing a size distribution on special graph paper (e.g., a log-log plot) and passing through some of the data points does not go through all the points of both the coarse and fine region. Thus there is no real justification for expressing the 100 percent size modulus k as an extrapolated point based on this line. Consequently there is no clear relationship between this modulus and some other measure of product distribution.

Instead of using a size modulus, a dimensionless mean product size is used in this report. The following definition was adopted:

$$\mu = \frac{x_2}{x_f} = \text{mean product size (dimensionless)}$$

where: $x_2 = \sum_{i=1}^{n} f_i x_i$ = mean product size[3/] (in),

---

[3/] The summation is actually from i = 1 to ∞; however for the smaller sizes the $f_i x_i$ terms are small and can be neglected.

---

x_i = average sieve size (mid-point of sieve class) (in),

$f_i = \dfrac{\text{weight in sieve class}}{\text{total weight of specimen}}$,

x_f = average feed size

$= \sqrt[3]{\dfrac{\text{weight of specimen}}{\text{density}}}$ [4/] (in).

[4/] The above definition of x_f is based on an assumed cubical shape because the specimens tended to be blocky. Other shapes, such as spheres, could also be used and would yield different factors in front of the cube root.

Bergstrom (1) conducted a series of tests at loading rates of 10^2, 10^3, 10^4, and 10^6 lbs/min. He concluded that the rate of loading had little effect on the energy - product relationship for glass spheres. However, he reported an increase in the energy required for fracture as the rate of loading was increased. He also investigated the magnitude and effect of kinetic energy on secondary breakage of glass spheres jacketed in steel and gelatin chambers. He noticed a significant effect of kinetic energy on product size distribution for two cases. He also concluded that the test environment, whether a steel crushing chamber or gelatin chamber, did not affect the average energy requirement for fracture of spheres of equal diameter.

In 1867, Rittinger postulated that the energy required for size reduction of a solid material would be proportional to the new surface area created in fragmentation. Because the new surface is directly proportional to the square of the new size and directly proportional to the average number of new particles which in turn is inversely proportional to the cube of the new size, mathematically Rittinger's hypothesis can be interpreted as follows:

$$E = K(1/x_2 - 1/x_1) \tag{15}$$

where

E = energy input per unit volume,
K = constant,
x_2 = final size,
and x_1 = initial size.

This hypothesis is simple to understand and several investigators have used it to interpret their experimental data or to improve upon this hypothesis.

In 1885 Kick postulated that equivalent amounts of energy should result in equivalent geometrical changes in the size of pieces of solids. This resulted in the equation

$$E = C \ln (x_1/x_2)$$

where

E = energy per unit volume,
C = constant,
x_2 = final size,
and x_1 = initial size.

In 1915, Gates (8) pointed out that Kick's hypothesis was at odds with rigorous experimental evidence. Ever since, no experimental data has been obtained to dispute this fact or to show that Kick's hypothesis is generally applicable to size reduction of rock-like materials.

What is frequently referred to as Charles' law (4) in the crushing and grinding literature (and which includes the above laws as special cases) was first proposed by Gilliland (16) as follows:

$$dE = -C \frac{dx}{x^n} \tag{16}$$

where dE is increment of energy, x is particle size, dx is increment of size, and C and n are constants. The integration of the above equation leads to the following expression:

$$E = \int_{x_1}^{x_2} [-C\, dx/x^n] = -C_1 \left[1/x_2^{\,n-1} - 1/x_1^{\,n-1}\right] \text{ for } n \neq 1, \tag{17}$$
$$= C \ln (x_1/x_2) \text{ for } n = 1.$$

Thus for n = 1 and 2, equation 17 takes the form of Kick's and Rittinger's laws of crushing respectively.

Bond (2) proposed that since neither Kick's nor Rittinger's hypothesis seemed valid for plant design work, an energy-size reduction relationship somewhere between the two was more applicable. The fundamental statement of Bond's mean index equation is derived from equation 16 with n = 1.5:

$$E = -C \int_{x_1}^{x_2} dx/x^{1.5} = K \left[1/x_2^{\,.5} - 1/x_1^{\,.5}\right] \tag{18}$$

Charles (4) pointed out that for a given cumulative distribution

$$y = f(x) \quad \text{or} \quad dy = f'(x)dx \tag{19}$$

where y = percent of weight less than size x, the energy dE required to reduce a weight, dy, from size x_m to x is

$$dE = \int_{x_m}^{x} [-C\ dx/x^n]\ dy \tag{20}$$

The energy E is then given by

$$E = \int_{x_o}^{k} \int_{x_m}^{x} (-C\ dx\ /x^{\ n})\ f'(x)dx \tag{21}$$

where k is the size modulus (described earlier in this section) and c is a constant. Charles showed that this reduces to the form

$$E = A/k^{n-1}$$

under various assumptions. This is similar to one of the forms used later in this report.

Oka and Majima (13) analyzed energy requirements in size reduction of irregular specimens. Their equation is as follows:

$$E_1 = K_1\ (x_1^{\ -6/\beta} - x_2^{\ -6/\beta}) \tag{22}$$

where: E_1 = total energy required in size reduction from feed size x_2 to product size x_1,
K_1 = constant,
β = constant.

For β = 12 or 6 this equation reduces to the empirical laws of Bond and Rittinger respectively; i.e., equation 22 is another form of Charles' law.

Intuitively, it is an appealing concept that the amount of energy utilized in the fragmentation process is proportional to the new surface area created (Rittinger's hypothesis). However, this concept does not hold in many cases due to the inherent heterogeneity and anisotropy of rocks and rock-forming minerals. A certain fraction of this energy is utilized in creating a network of cracks and flaws in new particles which were not inherent in the virgin material.

Thus, a summary of the whole situation of "laws" and equations is that theoretical equations tend to be approximate and essentially no more accurate than empirical equations.

Matrix-Vector Description of Single Event Comminution

In order to explain the results of the fragmentation analysis of this impact crushing investigation, it is necessary to relate the original sieve size of the specimens to the distribution of the various product sieve sizes obtained. One convenient method of doing this is to use the breakage matrix and the selection matrix. These relate the input (feed) to the output (product) and are explained in more detail below. Further details can be found in Broadbent and Calcott (3).

Let $a_1, a_2, \ldots, a_n$ be a decreasing geometric sieve size sequence with geometric ratio k, i.e., $a_{i+1} = ka_i$, with $k < 1$.

The breakage matrix, B, is defined by

$$B = (b_{ij}) = \begin{bmatrix} b_{11} & b_{12} & b_{13} & \cdot & \cdot & \cdot & b_{1n} \\ b_{21} & b_{22} & b_{23} & \cdot & \cdot & \cdot & b_{2n} \\ b_{31} & b_{32} & b_{33} & \cdot & \cdot & \cdot & b_{3n} \\ \cdot & \cdot & \cdot & & & & \cdot \\ \cdot & \cdot & \cdot & & & & \cdot \\ \cdot & \cdot & \cdot & & & & \cdot \\ b_{n1} & b_{n2} & b_{n3} & \cdot & \cdot & \cdot & b_{nn} \end{bmatrix}.$$

The b_{ij}'s relate feed fragments of size j to product fragments of size i, i.e., b_{ij} is that proportion of a fragment between a_{j-1} and a_j before breakage which falls between a_{i-1} and a_i after breakage.

The upper triangular portion of B (above the diagonal line) has all zero elements (i.e., $b_{ij} = 0$ for $j > i$) because a fragment cannot increase in size during comminution.

The selection matrix S is also used in this formulation. This matrix expresses the probability of selecting a set of size grade fragments. Thus S is defined as follows:

$$S = \begin{bmatrix} s_1 & 0 & 0 & \cdot & \cdot & \cdot & 0 \\ 0 & s_2 & 0 & \cdot & \cdot & \cdot & 0 \\ 0 & 0 & s_3 & \cdot & \cdot & \cdot & 0 \\ \cdot & \cdot & \cdot & \cdot & \cdot & & \cdot \\ \cdot & \cdot & \cdot & & \cdot & \cdot & \cdot \\ \cdot & \cdot & \cdot & & & \cdot & 0 \\ 0 & 0 & 0 & \cdot & \cdot & 0 & s_n \end{bmatrix},$$

where s_j is the proportion of the j-th size grade selected for breakage.

The input (or feed or frequency) vector $\vec{f}$ is defined as follows:

$$\vec{f} = \begin{bmatrix} f_1 \\ f_2 \\ \cdot \\ \cdot \\ \cdot \\ f_n \end{bmatrix},$$

where f_i is the proportion by weight of the feed fragments between the (i-1) and i-th grade size. The fraction f_n is the last sieve range measured. Consequently f_{n+1} is the fraction undersize and

$$f_1 + f_2 + \ldots + f_n + f_{n+1} = 1.$$

The output (product) vector p is defined in a similar fashion as follows:

$$\vec{p} = \begin{bmatrix} p_1 \\ p_2 \\ \cdot \\ \cdot \\ \cdot \\ p_n \end{bmatrix},$$

where p_i is the proportion by weight of the output fragments between the (i-1) and i-th sieve sizes.

Putting these definitions together, it is seen that the effect of a selection and breakage process on a feed distribution $\vec{f}$ is represented by

$$\vec{p} = [BS + (I - S)]\ \vec{f}$$

where BS $\vec{f}$ is the product selected and broken and (I-S) $\vec{f}$ is that part of the feed not selected for breakage. This simplifies to

$$\vec{p} = B\vec{f}$$

in the present case because S is the identity matrix I - all the specimens prepared are selected for comminution.

A further simplification of the B matrix is possible in many actual fragmentation processes and it was necessary to assume it to be valid for the present investigation. Let the matrix B be of such a nature that fragments of every size are broken in the same way and the product depends only on a scale factor. In other words, "scaling" is valid. Then, because the sieve sizes have been chosen to be in geometric ratio, it is seen that

$$a_i = a_1(k)^{i-1} \quad (k < 1;\ i = 1, 2, \ldots, n).$$

In this investigation $k = 1/\sqrt[4]{2}$.

Then it follows that

$$b_{ij} = b_{i-j+1,\,1} \quad (i \geq j),$$

so that the matrix B is completely determined by its first column and can be written in the new form:

$$B' = \begin{bmatrix} b_1 & 0 & 0 & \cdot & \cdot & \cdot & 0 \\ b_2 & b_1 & 0 & \cdot & \cdot & \cdot & 0 \\ b_3 & b_2 & b_1 & \cdot & \cdot & \cdot & 0 \\ \cdot & \cdot & \cdot & \cdot & & & \cdot \\ \cdot & \cdot & \cdot & & \cdot & & \cdot \\ \cdot & \cdot & \cdot & & & \cdot & \cdot \\ b_n & b_{n-1} & b_{n-2} & \cdot & \cdot & \cdot & b_1 \end{bmatrix} \quad \text{with } \vec{p} = B'\vec{f} \qquad (24)$$

where elements along any given down diagonal are all the same.

Writing out the matrix-vector multiplication, the following equations are equivalent to the more concise notation of the matrix-vector formulation:

$$\begin{aligned} p_1 &= b_1 f_1 \\ p_2 &= b_2 f_1 + b_1 f_2 \\ &\cdot \\ &\cdot \\ &\cdot \\ p_n &= b_n f_1 + b_{n-1} f_2 + \ldots + b_1 f_n \end{aligned}$$

The importance of the simplification of B to B' in this investigation is that all the non-zero elements of the matrix can be obtained by simply finding the elements of the first column (or last row).

In order to substantiate the assumption that the more general breakage matrix B can in fact be simplified as described above, it would be appropriate to start with the n different sizes of specimens and to fragment a group of each size to find out if the scaling is in fact valid. In practice it was found during the first series of drop tests that it was not possible, within the constraint on the number of tests that could be carried out, to obtain consistent results of the different size fragmentation products when more than one initial size set of irregular specimens was used. Disc specimens were also used and it appeared that more consistent breakage with fewer specimens could be obtained.

Thus one of the objectives of this investigation was to obtain the first column of the breakage matrix (equation 24). The values of the b_i's exhibited in appendices A1 - A6 are the values ultimately obtained. It is then assumed that the other columns of B' can be obtained from the b_i's as shown in equation 24.

DATA ANALYSIS

Drop Tests

Several series of drop tests were carried out to study the effects of size and shape so as to provide preliminary data for the design of impact pendulum experiments.

The first series of drop tests was designed to investigate the effects of shape and size on the value of λ, the exponential parameter in the exponential distribution:

$$Y = e^{-\lambda x}$$

During this phase of the investigation, the exponential law was being used as a base law for the analysis. From this experiment and later drop tests, it was found that the exponential distribution was not a good model.

As a basis for this preliminary investigation, random shaped specimens were used to simulate the feed vector in which all the specimens have the same initial sieve size. Sixty-four tests were conducted on specimens varying between 500 and 1,000 gm to select the number of tests in the final test series.

From sieve analysis results and calculated λ values, it was concluded that a minimum of 30 tests would be required for each test situation to obtain reproducible results for estimating a composite λ. This value of 30 was a compromise between statistical estimation of the variability of the mean, and a need to keep the total number of tests down to a reasonable total. Sequential testing was also considered in order to keep the number of samples to a minimum; however it was felt that the average sample number in a sequential test would have to be interpreted as 30 so that no savings would be achieved.

Data analysis of the first 64 tests also revealed a high scatter in the value of the distribution parameter λ. Therefore, a second test series was designed to investigate the effect of shape and size on test results.

To investigate the shape factor in this second test series, the specimens were divided into three groups based on their geometrical configuration - equidimensional, elongated, or flat. To incorporate the effect of volume, the weight of specimens in each category was varied from 100 to 7,000 gm. All specimens were dropped from a constant height of 35 ft.

Results of the experiments indicated a high scatter in the individual values of λ. The data also indicated that equidimensional specimens show a lower probability of breakage than do elongated specimens which, in turn, show a lower probability of breakage than the flat specimens. The larger specimens also showed higher probability of breakage than the smaller specimens for comparable shapes. These results are summarized in table 2.

The values of λ for each weight class also increase as the probability of breakage increases. This is to be expected because $1/\lambda$ is the mean of the exponential distribution; i.e., the average size decreases as the probability of breakage increases.

In the final series of drop tests, one hundred and eighty specimens (ninety of Wausau quartzite and ninety of anorthosite) were fragmented. Thirty of each rock type were dropped from heights of 25, 30, and 35 ft. The fragments from each specimen that broke were then sieved to obtain the weight of fragments of each specimen in each sieve class.

To analyze the sieve data, the cumulative sieve percentages were obtained and plotted for each specimen that broke - all plots for one drop height being shown on the same graph. It was evident from these three graphs that the sample-to-sample variation was so great that taking an average (forming a composite) of all the samples (number of samples = $n \leq 30$) would yield a better description of all the samples and consequently show better the general trend of the fragmentation process.

Consequently the next step taken was to form a composite distribution by adding the n individual weights together for each sieve class and then finding the percentage and cumulative percentage for each sieve class. This was carried out for each of the three drop heights (see Figs. 4a and 4b).

Another method of forming a composite distribution for each drop height is to find the fraction by weight for each individual specimen for each sieve class and to average these n fractions for each sieve class.

The first composite distribution described above is equivalent to the distribution that would be obtained by breaking all the original size rocks together. This, in effect, simulates a multiple rock single-event crushing process. The second distribution described above is the statistical distribution that it would be natural to form. Thus both distributions are logical from different points of view. As it turns out, both distributions are very nearly the same, i.e., the overall percentage in each sieve class is approximately the same for either distribution. In this investigation both distributions were calculated, but only the former is shown in the various figures.

TABLE 2. - Experimental data from low impact velocity drop tests

Shape	Specimen size (small)		
	Number of replications (includes both broken and unbroken specimens)	λ for average weight of 800 gm (approx)	Probability of breakage
Equidimensional	47	0.060	0.618
Elongated	49	.114	.835
Flat	37	.174	.975
	Specimen size (large)		
	Number of replications	λ for average weight of 1,600 gm (approx)	Probability of breakage
Equidimensional	32	0.054	0.876
Elongated	27	.089	.965
Flat	46	.116	1.000

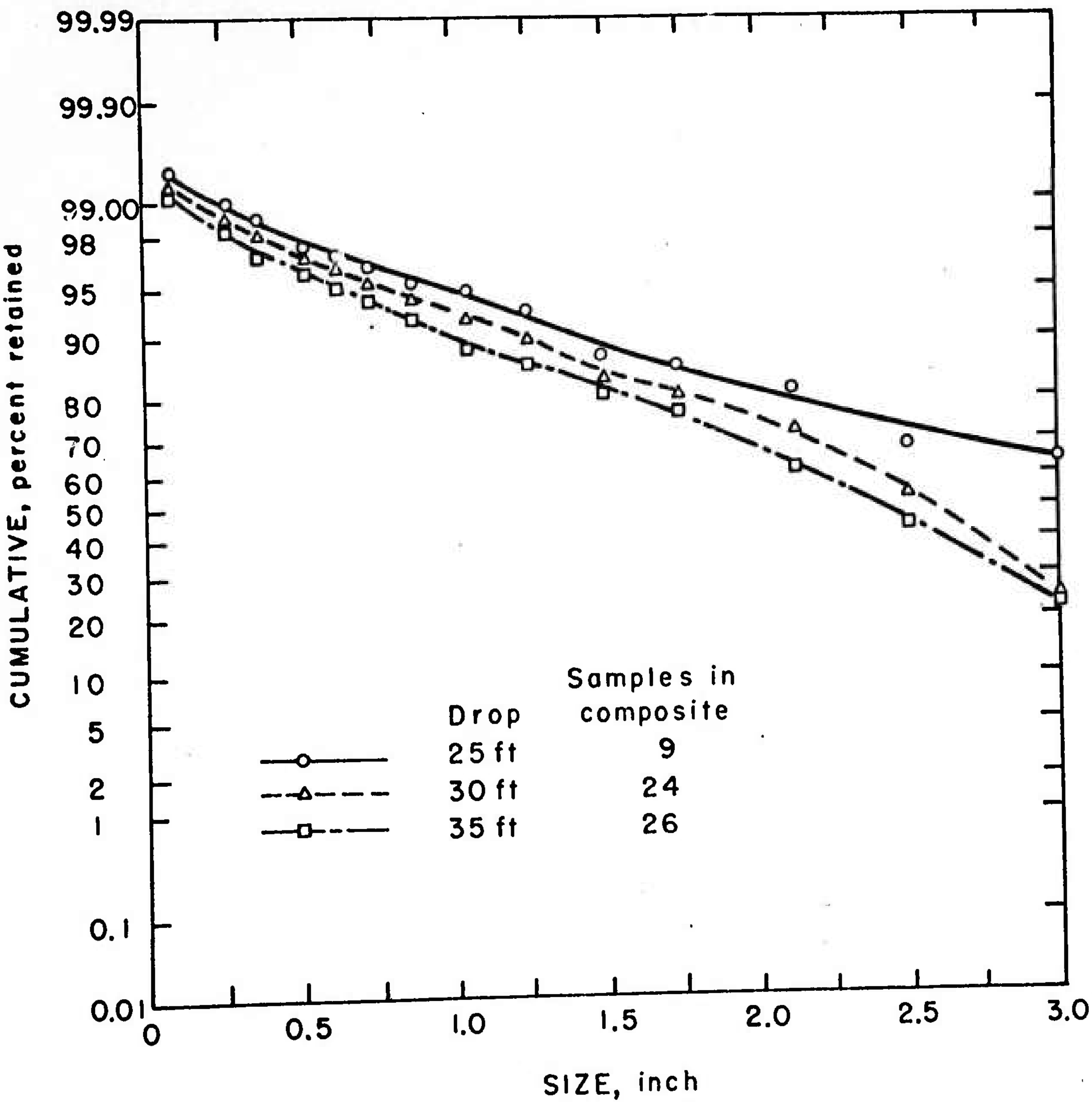

Figure 4a. Curves fitted to cumulative size distributions of composite data from drop tests of irregular Wausau quartzite specimens.

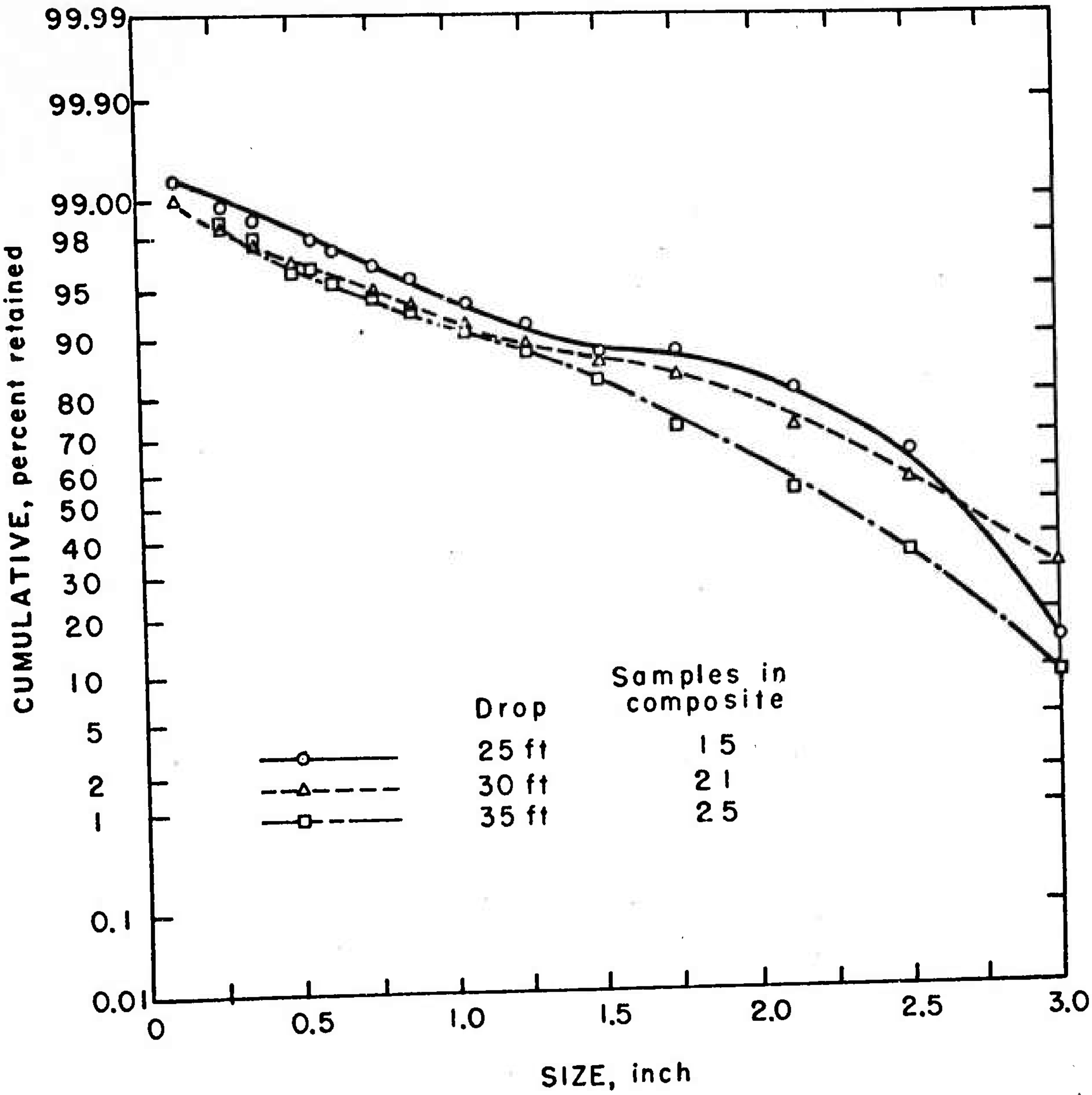

Figure 4b. Curves fitted to cumulative size distributions of composite data from drop tests of irregular anorthosite specimens.

The final step was to statistically analyze and plot these cumulative results to find which distribution fitted best. Three distributions were used - the power law distribution, the exponential distribution, and the normal distribution. It turned out that the normal plots had the best correlation coefficient, but this was not evident until the following complication had been resolved.

The composite set of data points for a given drop height when plotted on normal paper yielded a set of data points which resembled a straight line segment and a slowly bending curve (see Figs. 4a and 4b).

Consequently it was decided to separate the sieve data into two groups - "fine" and "coarse." The cut-off point was selected visually as approximately 1.05 inches for the anorthosite and 1.25 inches for the Wausau quartzite. These two groups were then recompiled (renormalized) separately and each group was plotted separately. Thus where there were three "dual" segment plots before, there are now six separate sets of points and lines for each rock type. These are shown in figures 4c, 4d, 4e, and 4f. These last six lines (on normal paper) were fitted by the least squares procedure. The correlation coefficient for each line, showing goodness of fit, is also shown on each figure.

Note that each curve or straight line in figures 4a-4f was plotted for a given drop height. This is equivalent to plotting for a given specific crushing energy because specific crushing energy is proportional to drop height:

$$E_c = \frac{W \cdot h}{(W/\rho)} = \rho h$$

where: E_c = specific crushing energy (ft lb/ft^3),
ρ = rock density (constant) (lb/ft^3),
W = specimen weight (lb),
h = drop height (ft).

Impact Pendulum Test

For each separate impact pendulum test, calculations were made of the rebound height of the second (rebound) pendulum by two methods. The rebound heights by the two methods respectively were calculated as follows:

First method:

$$h = R - \sqrt{R^2 - x^2} \tag{25}$$

where: h = rebound height (in),
R = length of pendulum wire (from pivot point to center of gravity of rebound pendulum) (in),
x = measured horizontal travel of rebound pendulum (in).

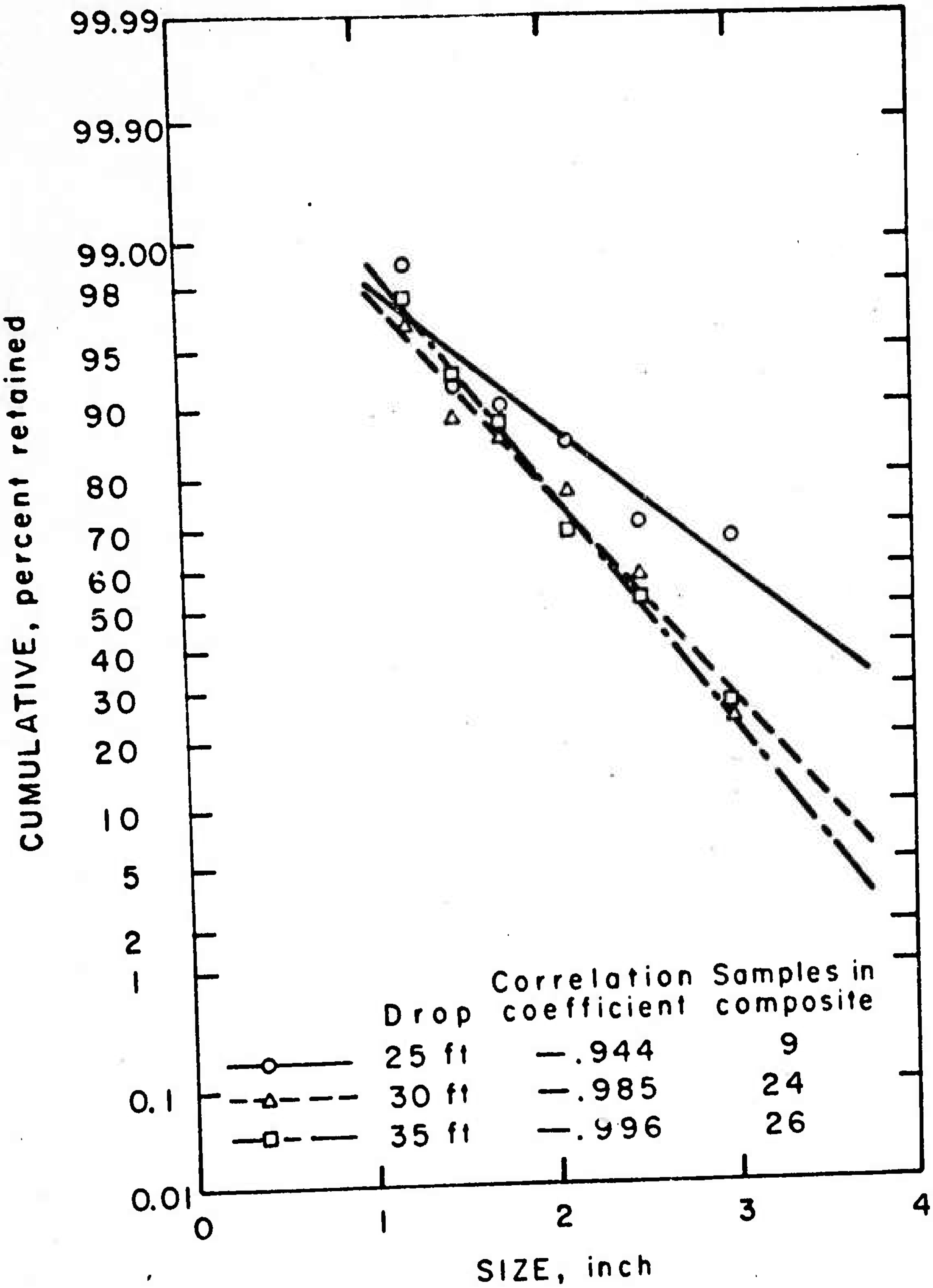

Figure 4c. Normal curves for fragments > 1.25 in fitted to cumulative size distributions of composite data from drop tests of irregular Wausau quartzite specimens.

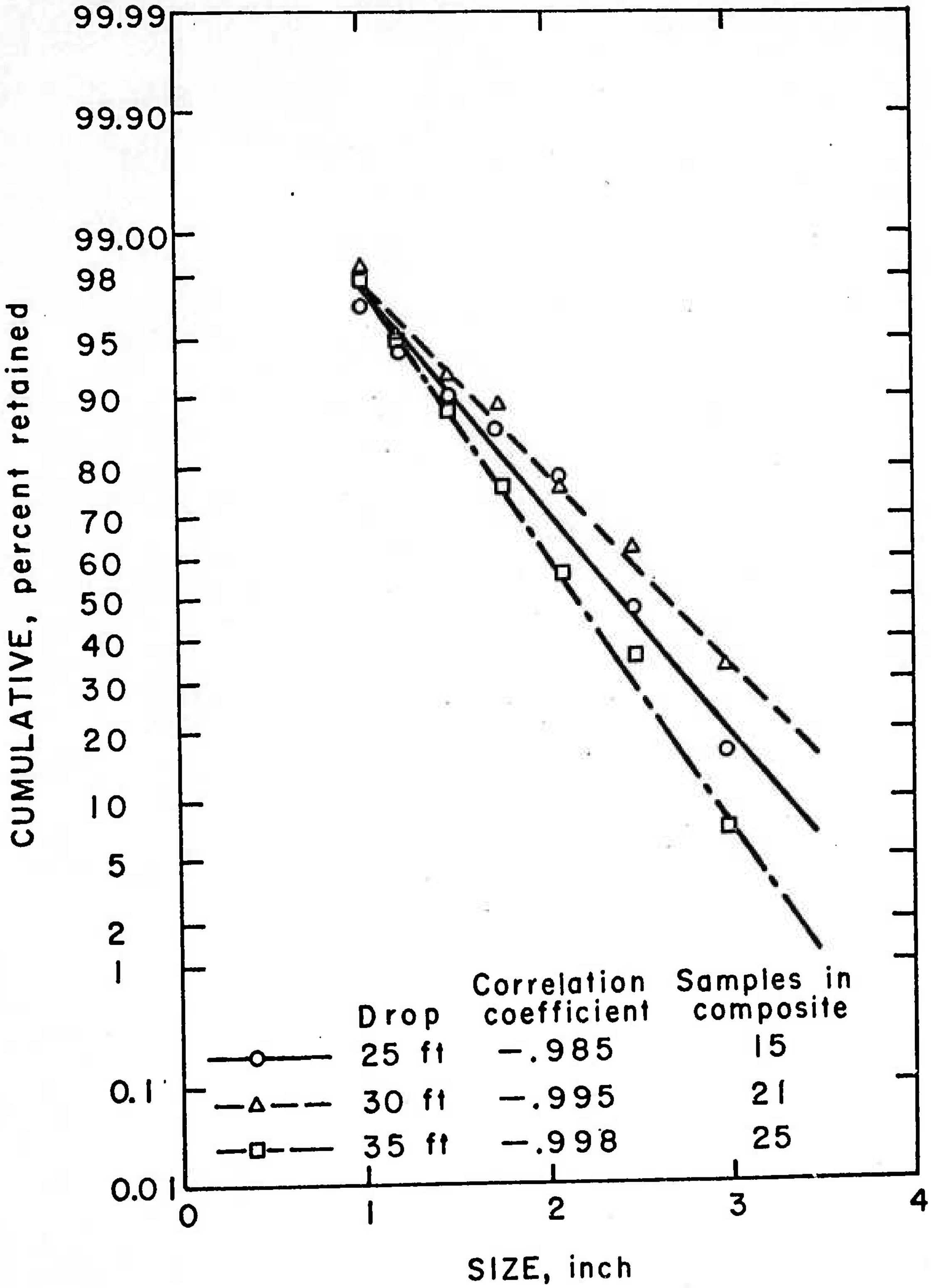

Figure 4d. Normal curves for fragments > 1.05 in fitted to cumulative size distributions of composite data from drop tests of irregular anorthosite specimens.

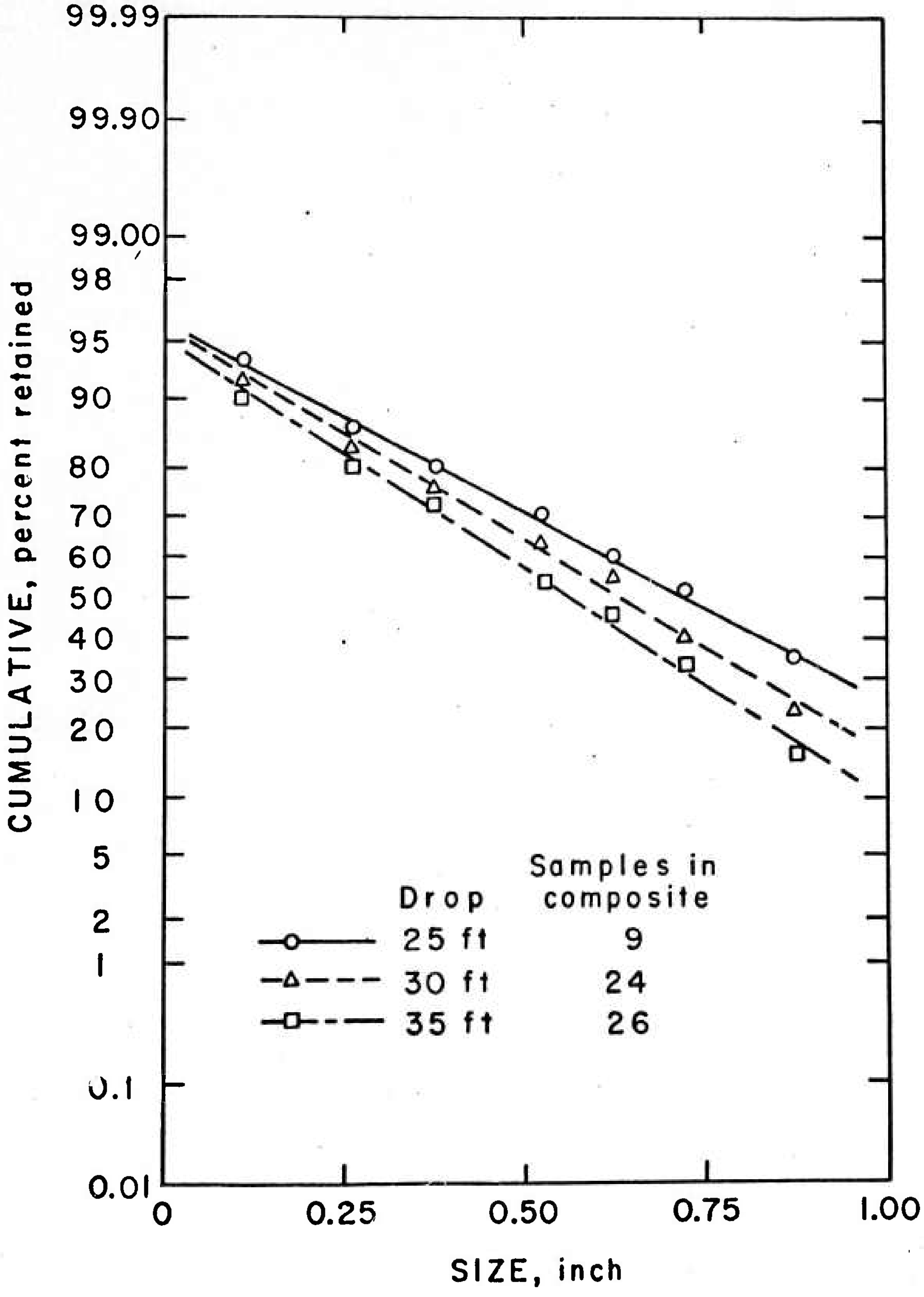

Figure 4e. Normal curves for fragments > 1.25 in fitted to cumulative size distributions of composite data from drop tests of irregular Wausau quartzite specimens.

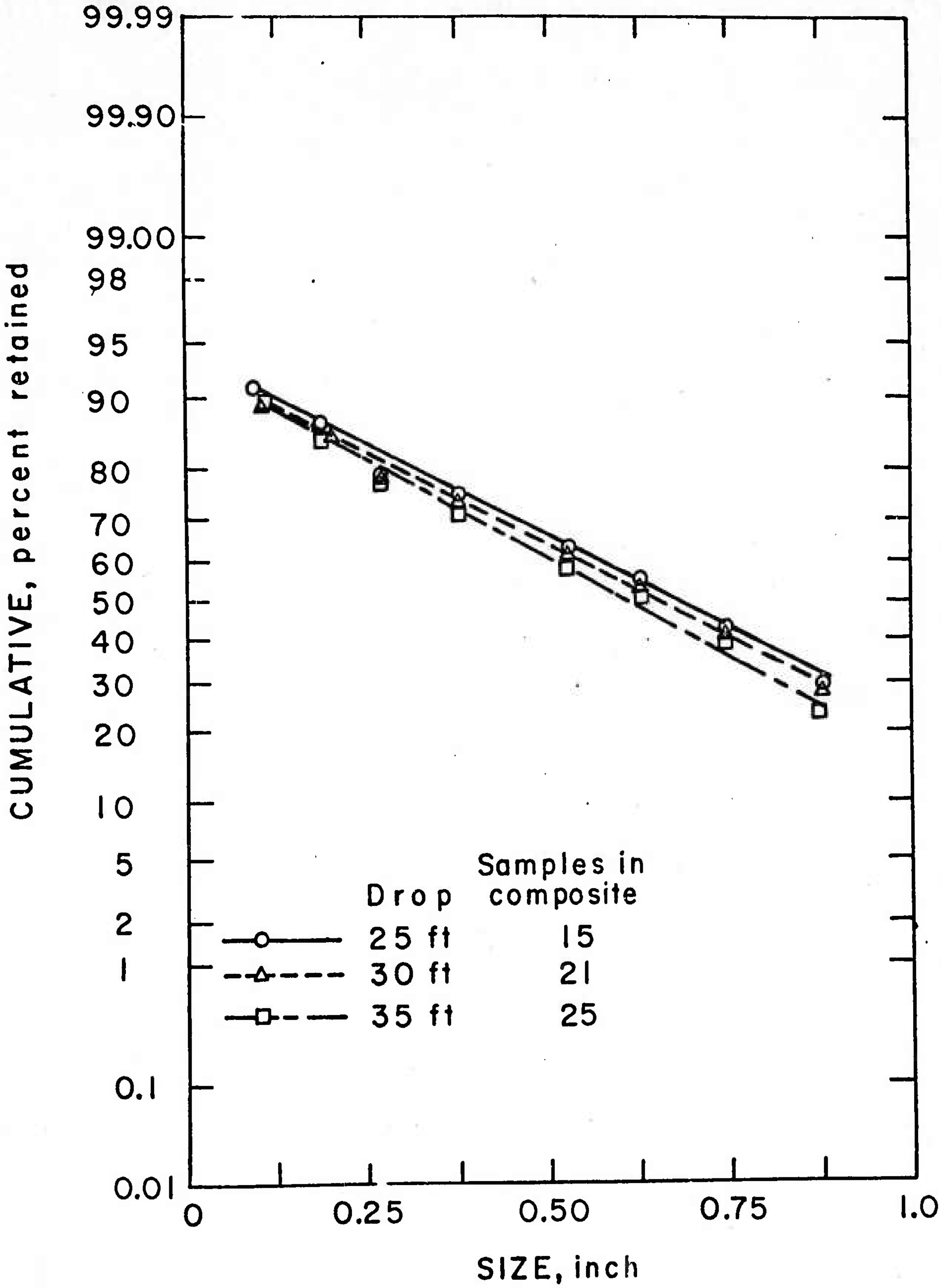

Figure 4f. Normal curves for fragments > 1.05 in fitted to cumulative size distributions of composite data from drop tests of irregular anorthosite specimens.

Second method:

$$V = \frac{\Delta y}{\Delta t} \tag{26}$$

where

V = rebound velocity (ft/sec),
Δy = 1/12 (ft),
= width of black shield attached to pendulum,
Δt = time (sec) for shield to travel 1/12 ft (measured by timer).

Calculations from the photocell/timer indicated inconsistent velocity values. This was probably caused by fluctuations beyond control in background lighting which affects the two trigger points that start and stop the Δt time interval on the digital counter. Consequently these calculations were not used in the analysis.

Calibration of Impact Pendulum

It was essential to calibrate the impact pendulum for two reasons, (1) to determine the energy lost in the system and (2) to check the alignment of the pistons by verifying for given input energies the repeatability of the piston velocities. High-speed photography was used to determine the relative motions of the first pendulum, first piston, second piston, and second pendulum with no specimen present. Five high-speed photographs were made of these moving parts. It was found that after impact the latter three parts remained in contact with each other and travelled as one unit for a distance of about 1 in. After this, the second pendulum separated from the two pistons because of the roller bearing friction on the pistons. The first pendulum approximately stopped after impact. Since the latter three parts remained in contact with each other briefly after impact, it was assumed that the velocities of all three were the same.

In order to calculate the mechanical energy lost, E_{L_1}, the following energy balance relationship is used (see sketch below):

$$\text{Energy in} = \text{Energy out} + \text{Energy lost},$$

or

$$W_1 h_1 = 1/2\left(\frac{W_2}{g} + \frac{W_3}{g}\right) V_2^2 + W_4 h_4 + E_{L_1}, \tag{27}$$

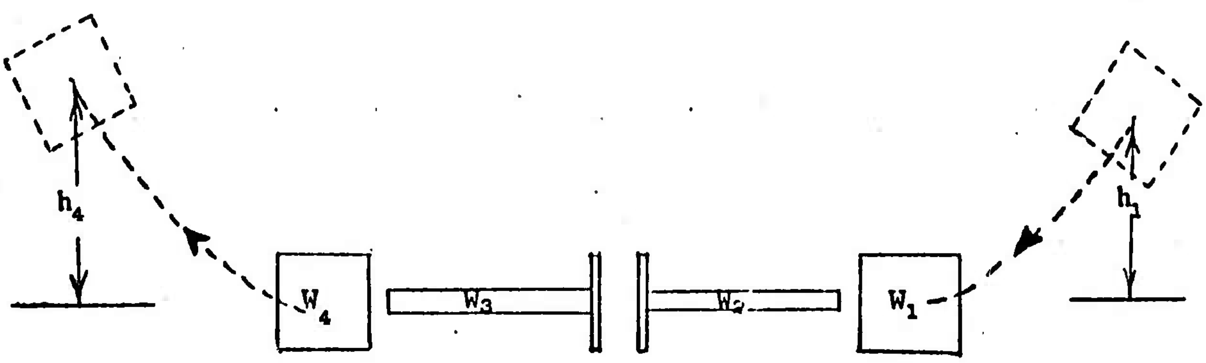

where

W_1 = weight of first pendulum,
h_1 = release height,
W_2 = weight of first piston,
W_3 = weight of second piston,
V_2 = velocity of first and second pistons,
W_4 = weight of second pendulum,
h_4 = height to which second pendulum ascends,
E_{L_1} = energy lost in friction, heat, vibration, etc. with no specimen between pistons.

Equation (27) can be rewritten as

$$E_{L_1} = W_1 h_1 - W_4 h_4 - 1/2 \left(\frac{W_2}{g} + \frac{W_3}{g}\right) V_2^2 \tag{28}$$

The numerical values for the input energy, W_1h_1, for the calibration output energy, $1/2 \left(\frac{W_2}{g} + \frac{W_3}{g}\right) V_2^2 + W_4h_4$, and for energy lost, E_{L_1}, are given in Table 3 (see equation 28).

Calculation of Crushing Energy

High-speed photographs of specimen fragmentation runs indicated that all the moving parts (first pendulum, first piston, specimen, second piston, and second pendulum) remain in contact immediately after impact. When the specimen is held between the two pistons, the motion of the first pendulum is different than in the calibration calculations (where no specimen was present) in that it moves along with the other parts. Thus, to obtain the crushing energy utilized in breaking the specimen, it was only essential to determine the velocity of the second pendulum immediately after impact both with and without a specimen held between the pistons.

The energy balance when the specimen is present (see sketch below) is given by the following equation:

Energy in = Energy out + Crushing energy + Energy lost,

or

$$W_1 h_1 = 1/2 \left(\frac{W_1}{g} + \frac{W_2}{g} + \frac{W_S}{g} + \frac{W_3}{g}\right) V_3^2 + W_4 h_5 + E_c + E_{L_2}\,, \tag{29}$$

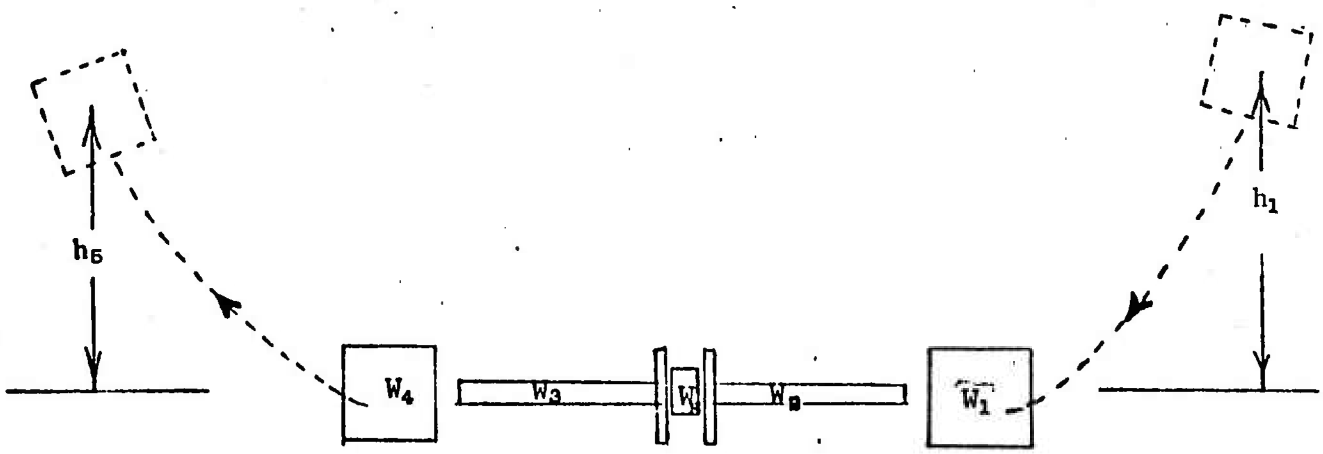

TABLE 3. - Energies involved in calibration for different input energies.

Release height position (see figure 2)	Release height, in	Input energy $W_1 h_1$ ft-lb	Calibration output energy ft-lb	Energy lost, E_{L1} ft-lb
3	7.0	95.	67.	28.
C	12.1	164.	122.	42.
2	16.5	223.	160.	63.
B	21.5	293.	220.	73.
1	26.9	365.	271.	93.
A	33.6	455.	355.	101.

where

W_1, W_2, W_3, W_4, and h_1 are defined above,

W_s = weight of specimen,

V_3 = velocity of first and second pistons,

h_5 = height to which second pendulum ascends,

E_c = crushing energy,

E_{L_2} = energy lost in friction, heat, vibration, etc. with specimen present.

It is assumed that

$$E_{L_1} \approx E_{L_2} \text{ .}$$

Hence when equations (27) and (29) are set equal, the following expression[5/]

[5/] Note also that $W_4h_4 = 1/2 \frac{W_4}{g} V_2^2$ and $W_4h_5 = 1/2 \frac{W_4}{g} V_3^2$.

for crushing energy, E_c, is found:

$$E_c = 1/2 \left(\frac{W_2}{g} + \frac{W_3}{g}\right) V_2^2 - 1/2 \left(\frac{W_1}{g} + \frac{W_2}{g} + \frac{W_s}{g} + \frac{W_3}{g}\right) V_3^2 + W_4h_4 - W_4h_5. \quad (30)$$

The input energy W_1h_1 is the same during both calibration runs and specimen runs from a given release height; consequently, this parameter does not affect the value of crushing energy E_c and so does not appear in equation 30.

A computer program was used to calculate the calibration output energy, and crushing energy, and the specific crushing energy for each specimen and averages of these for each release height (input energy) and rock type used in the testing. (See DATA ANALYSIS, Impact Pendulum Test section.)

To facilitate analysis, four digital computer programs were used to analyze the recorded test data and sieve data obtained from the fragmented specimens.

The first program used sieve data to calculate the following: cumulative data for each resultant fragment distribution, the composite distribution from a number of these individual fragment distributions, and the means and standard deviations of the individual and composite distributions. All the sieve data from the 270 fragmented irregular (-3.5 + 3.0 in) specimens and the 150 disc (2 in diameter x 1 in) specimens of the three rock types were run using this program.

The second program was used to calculate the rebound velocity of the rebound pendulum from both a photocell/timer method and a distance measuring method. (This was discussed in the Impact Pendulum Test Apparatus section.)

The third computer program was used to calculate the calibration output energy, the crushing energy, and the specific crushing energy (crushing energy/specimen volume) for each specimen and averages of these for each release height (energy input) and rock type used in the testing. (The equations for calculating these energies were developed in the Experimental Program section.) This data is summarized in appendices B1 - B24.

The fourth program was used to fit various functions to the sieve data. The six distribution functions given in equations 9-14 were used. The fitted normal distributions are shown in figures 5a, 5b, 5c, 5d, 5e, and 5f. The same method of combining individual tests into a composite distribution is used as was used to obtain the composite distribution for the drop tests.

The output from these computer programs was quite extensive and consequently is not totally reproduced in this report. Instead, a summary of the most pertinent information is given in appendices B1 - B24 and C1 - C6.

Included in appendices B1 - B24 are specimen weight, mean product size, standard deviation of product, specimen output energy (from pendulum output velocity), crushing energy (that portion of the input energy actually utilized in crushing), specific crushing energy (crushing energy per volume of specimen), averages of the above parameters, and mean and standard deviation of the composite fragment data. (Composite data are obtained by pooling the weights of fragments in given sieve classes from all the products listed in that particular appendix.)

Because the specimens, particularly the irregular ones, were of different sizes and weights even though they were of the same sieve size, it was necessary to compare the mean product size and the product standard deviation with an original size as follows: The original weight of the specimen was converted to volume by dividing by the rock density, and the cube root of this volume was considered to be the specimen size. Dividing this value into the values of the mean and standard deviation yielded a dimensionless mean and standard deviation. These dimensionless versions of the mean and standard deviation are also given in appendices B1 - B24. The dimensionless mean is also used in several figures.

Included in appendices C1 - C6 are summary data relating to various functions that were fitted to the cumulative sieve data. The columns headed A and B give the intercept and slope respectively of the fitted function in the form where it has been found as a straight line, (e.g., $R = \exp(\lambda x)$ becomes $y = \log R = \lambda x$, so that $A = 0$ and $B = \lambda$).

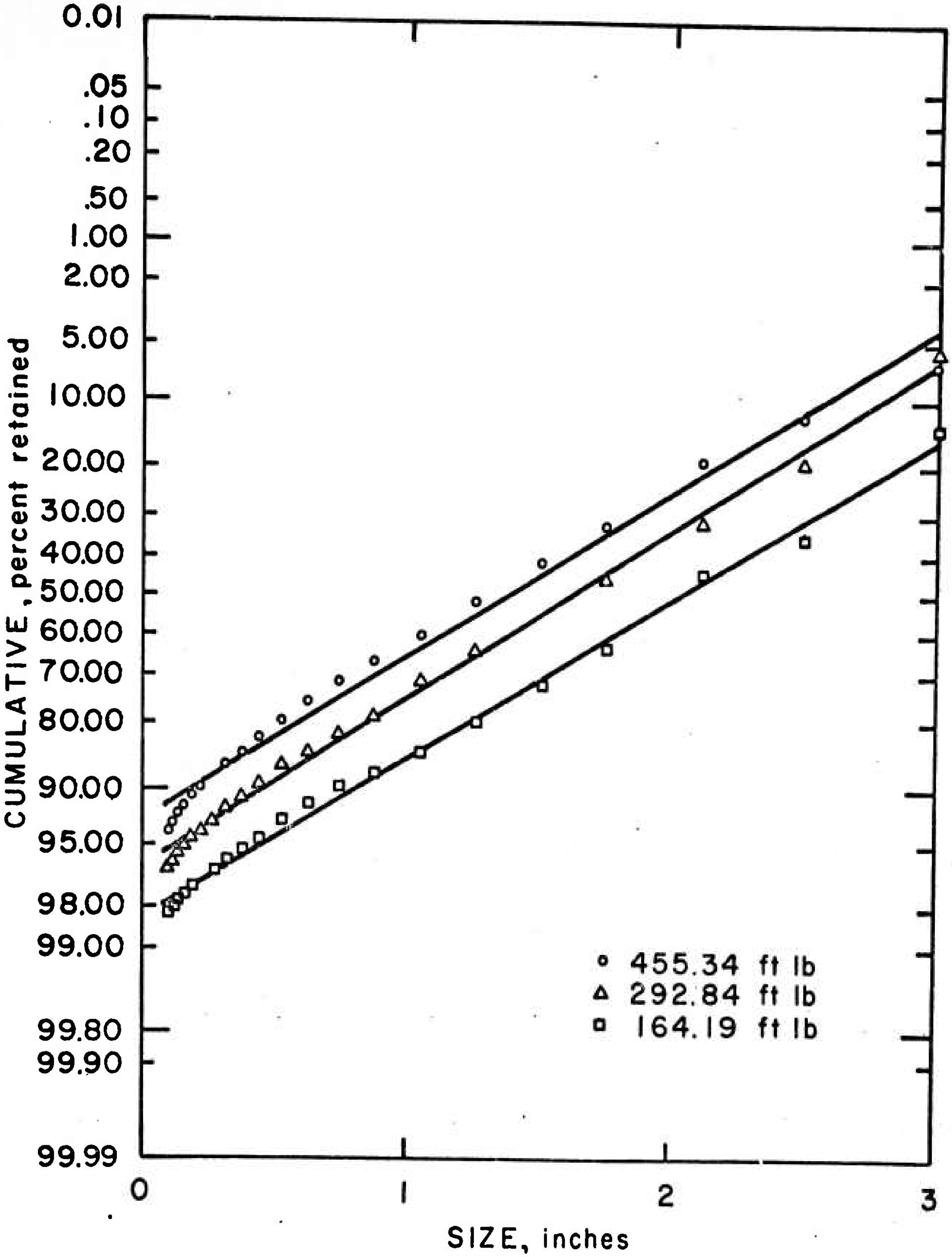

Figure 5a. Normal curves fitted to cumulative size distributions of composite data from impact tests of irregular Wausau quartzite specimens.

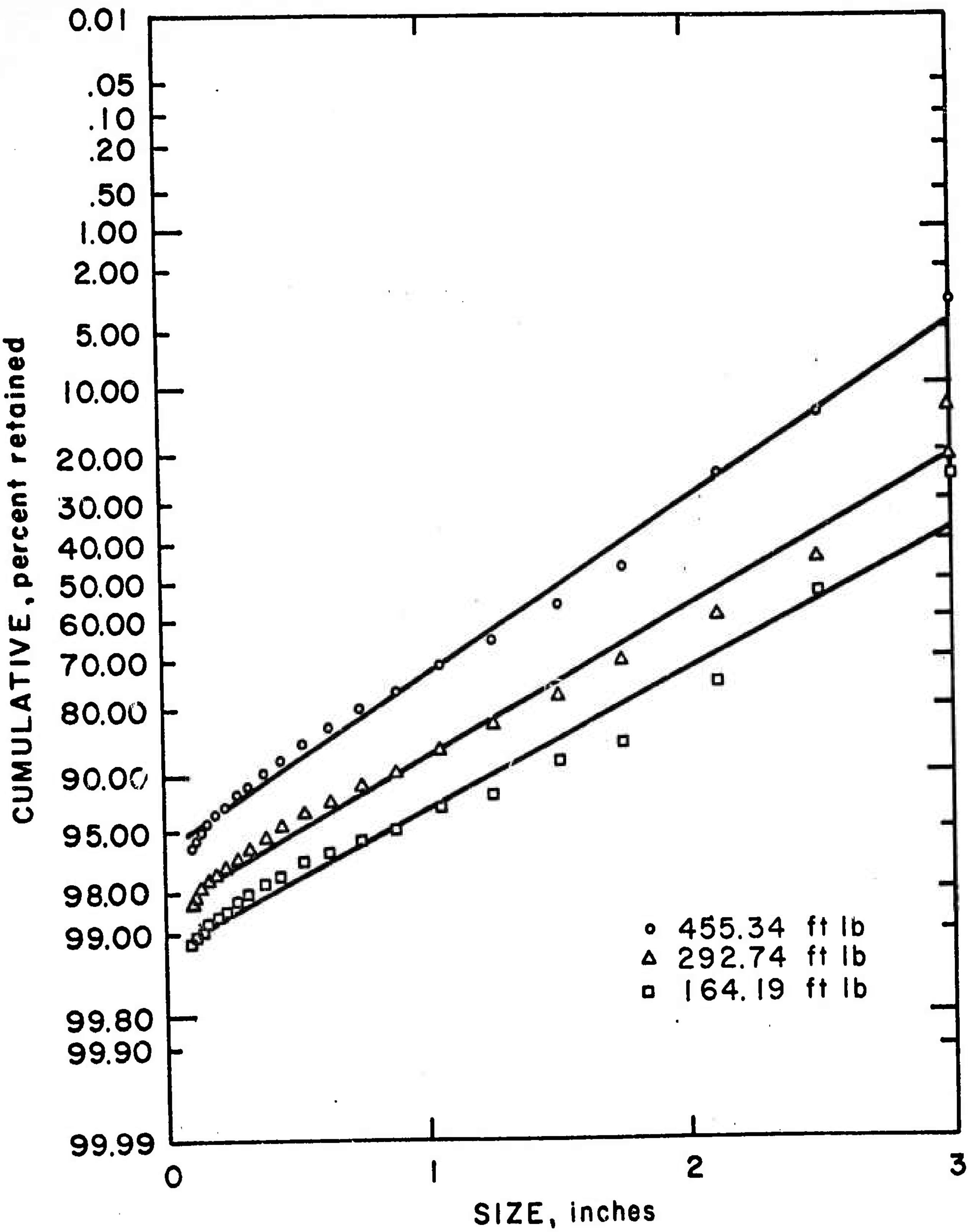

Figure 5b. Normal curves fitted to cumulative size distributions of composite data from impact tests of irregular anorthosite specimens.

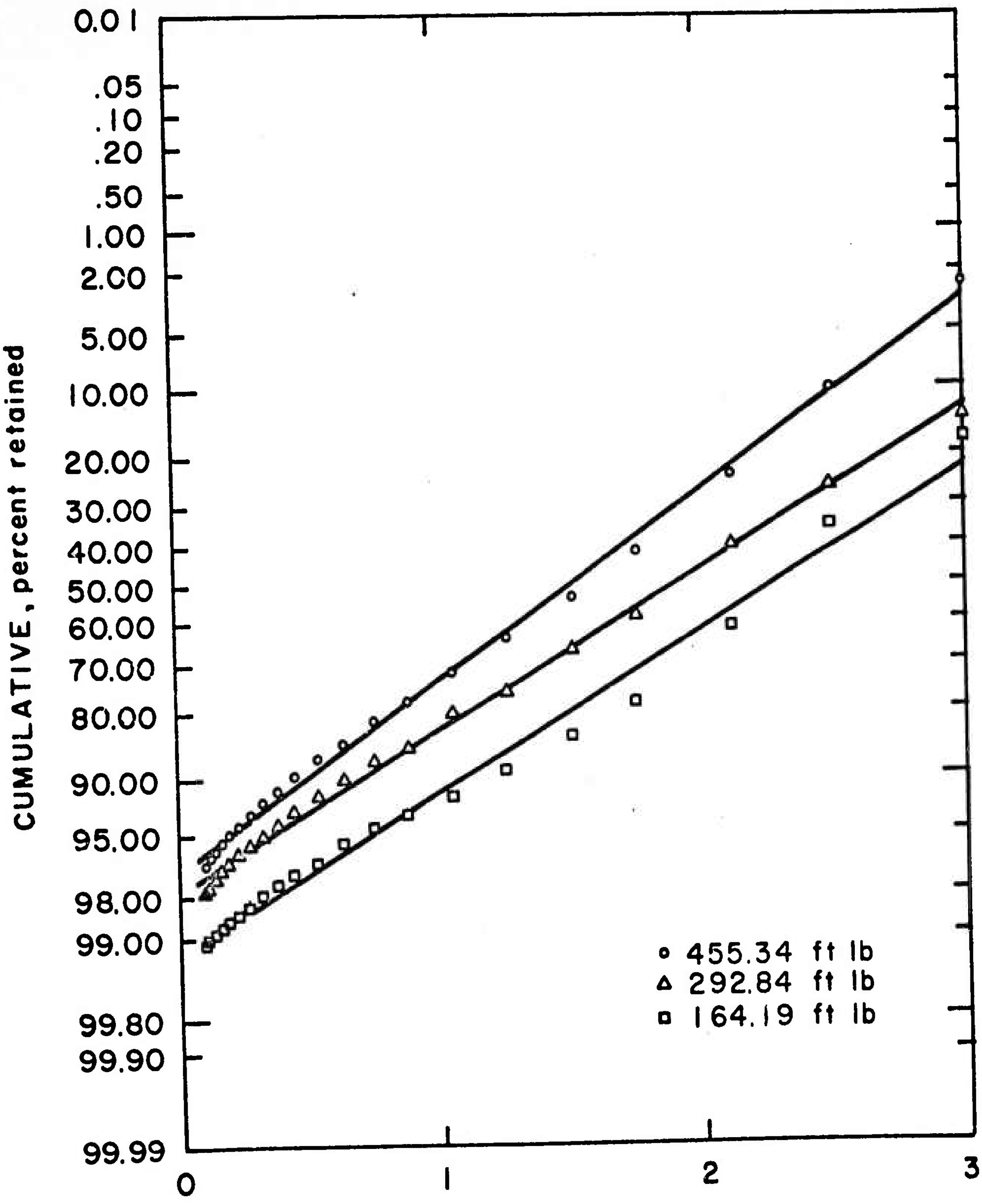

Figure 5c. Normal curves fitted to cumulative size distributions of composite data from impact tests of irregular Felch marble specimens.

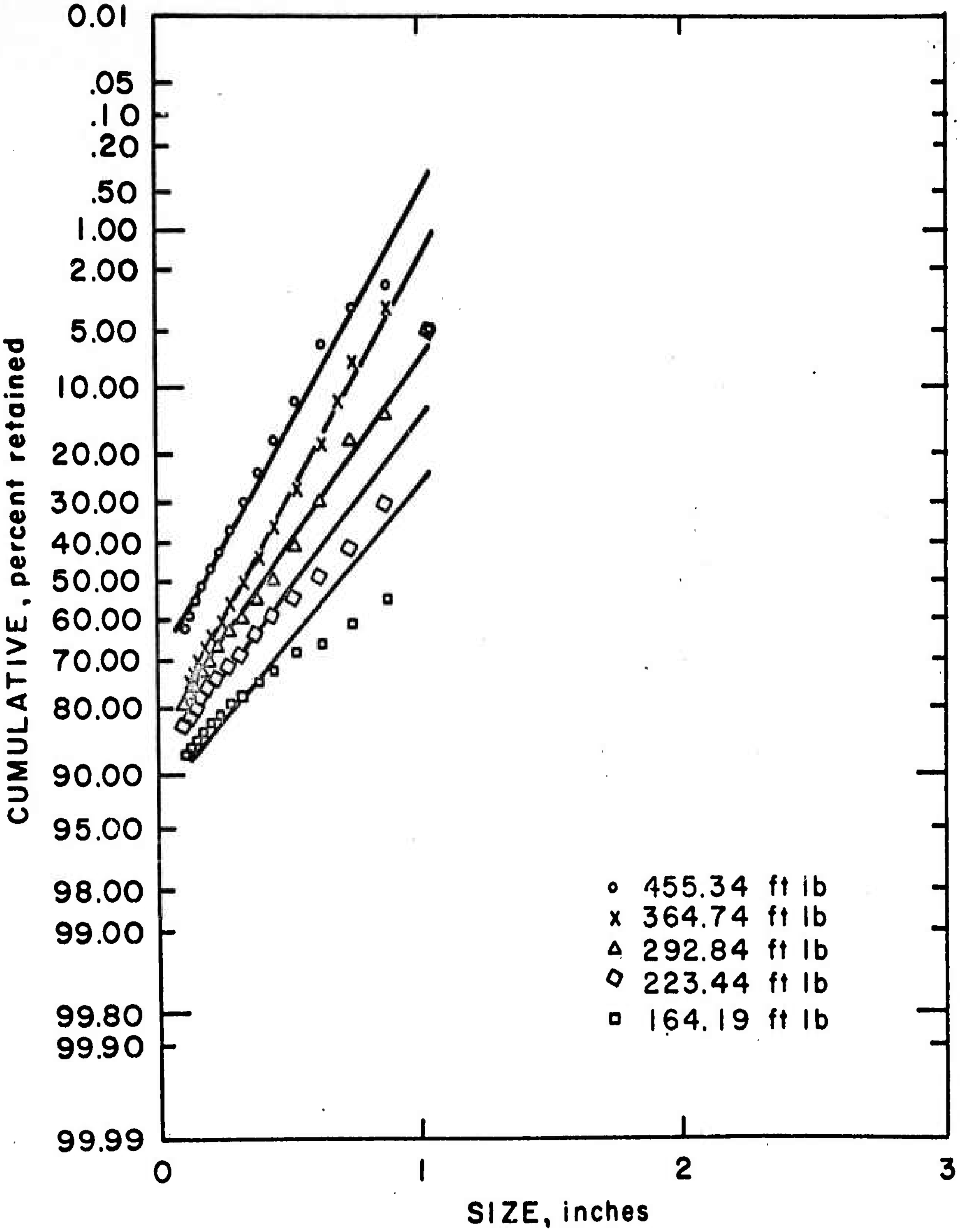

Figure 5d. Normal curves fitted to cumulated size distributions of composite data from impact tests of disc Wausau quartzite specimens.

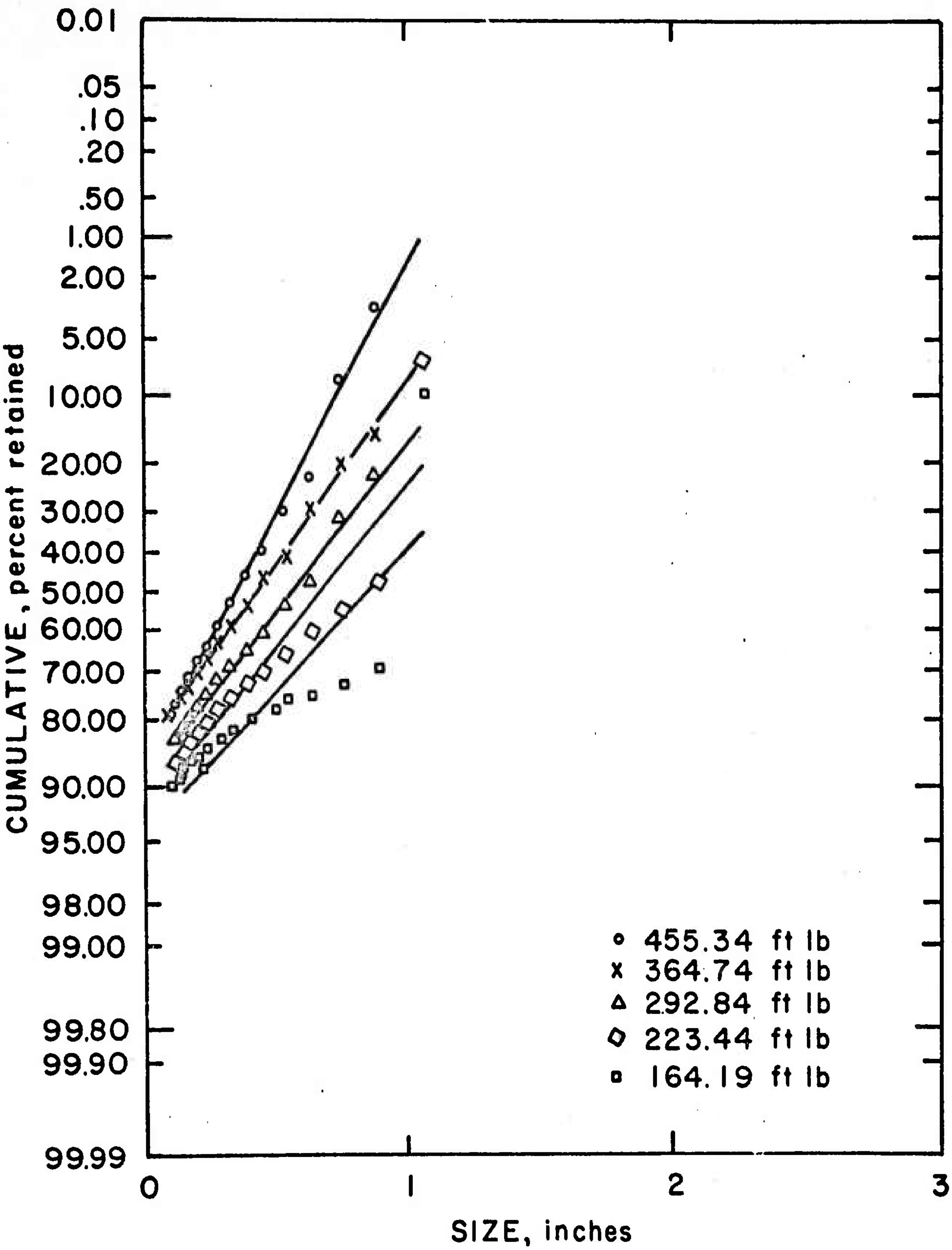

Figure 5e. Normal curves fitted to cumulative size distributions of composite data from impact tests of disc anorthosite specimens.

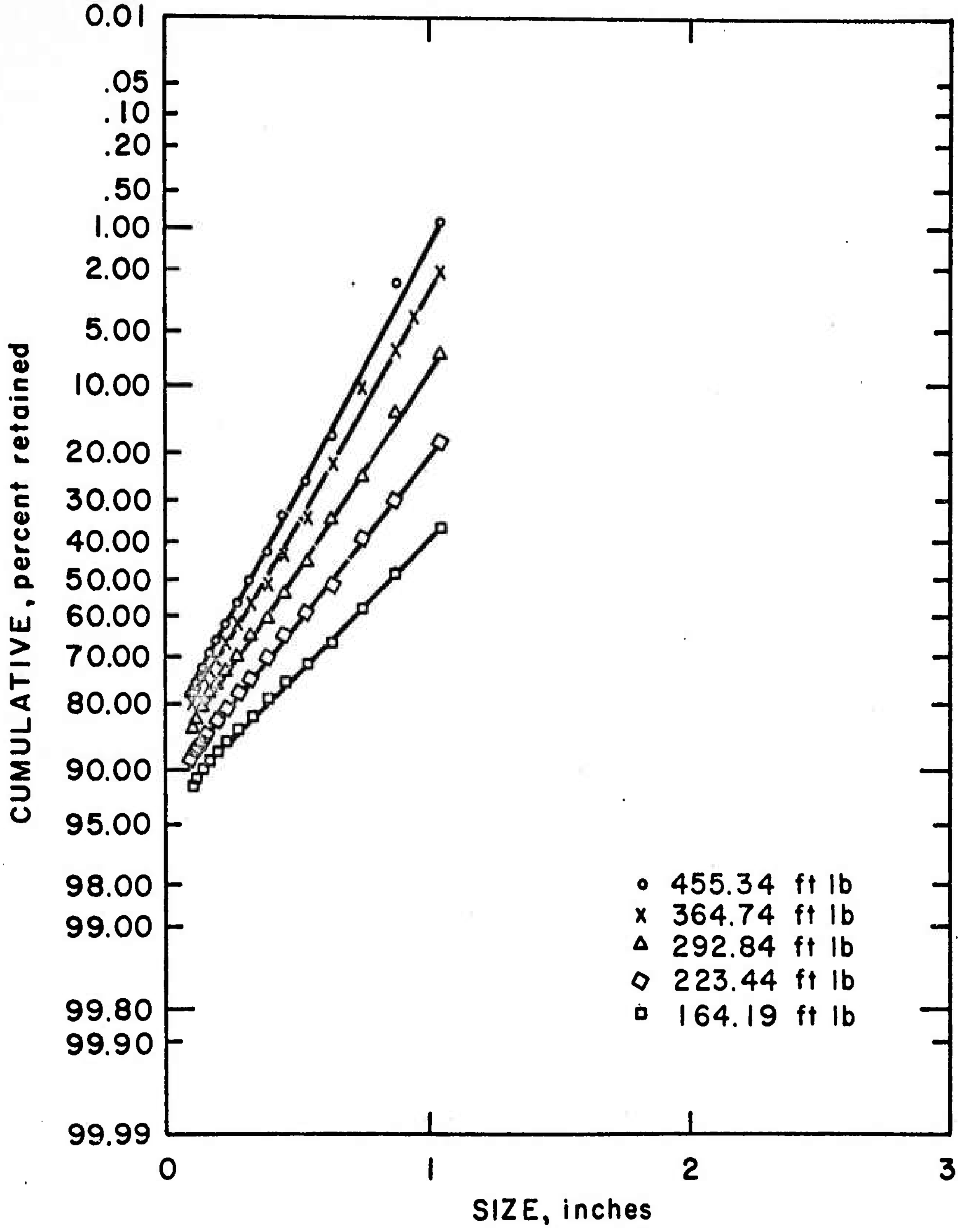

Figure 5f. Normal curves fitted to cumulative size distributions of composite data from impact tests of disc Felch marble specimens.

The other two columns show the coefficient of correlation and the coefficient of determination. The correlation coefficient shows how well the line fits the transformed data points, and the coefficient of determination shows how well the fitted function fits the original points. Comparison of the various correlation coefficients is usually taken to indicate the best fit of those functions considered. The normal function generally yields the best fit and the power curve or the log Weibull the second best fit in these appendices.

Inasmuch as the normal was taken to be the best fit, it was desirable to make a check on the suitability of the normal, so a separate comparison between the mean and standard deviation of the product as calculated from the normal distribution and as calculated from the composite sieve data (also shown in appendices B1 - B24) was made. Table 4 provides the data organized for comparison. Generally the composite mean is slightly greater than the normal mean, but the composite standard deviation is less than the normal standard deviation. Thus it appears that the normal is a reasonable fit to the data.

In this investigation, the first attempt at relating specific energy and mean product size followed along the lines of the work of Bergstrom (2) or Charles (4), as discussed in the Fragment Distributions section. The function used was the following hyperbolic (or power law) function

$$E/V_o = a/\mu^b \tag{31}$$

where

E = energy (ft-lb)
V_o = initial specimen volume (ft^3),
a, b = constants related to the breakage process and the rock type,
$\mu = X_p/X_f$ = dimensionless mean product size,
X_p = mean product sieve size (in),
X_f = initial specimen size (in) = $V_o^{1/3}$ (V_o in in^3).

The mean product size was used rather than the 100 percent modulus (the curve fitted value of the ratio of the largest product size to the initial specimen size) because the 100 percent value would have been between 0.9 and 1.0 in all cases, making it difficult to distinguish between differing product size results resulting from different input energies.

The values for a and b were determined by a digital computer least squares fit of the power law. These values are summarized in a brief table included in figure 7. Both figures 6 and 7 show the power law fitted to the data points, figure 6 on rectangular graph paper and figure 7 on log-log paper. The lines in figure 7 show excellent fits to the data points, particularly in the disc specimen cases. Note that in figure 7, a is the intercept, i.e., the value of E/V_o when $\mu = 1$ (or

TABLE 4. - Comparison of mean and standard deviation as calculated from the normal distribution and from composite sieve data

Material	Release height	Shape	Mean = μ (in.) Normal	Mean = μ (in.) Composite	Standard Deviation = σ (in.) Normal	Standard Deviation = σ (in.) Composite
Felch Marble	C	irregular	2.304	2.264	0.939	0.724
Felch Marble	B	irregular	1.931	1.958	0.951	0.851
Felch Marble	A	irregular	1.522	1.612	0.806	0.745
Wausau quartzite	C	irregular	2.030	2.052	0.967	0.835
Wausau quartzite	B	irregular	1.631	1.713	0.910	0.838
Wausau quartzite	A	irregular	1.387	1.476	0.937	0.852
Anorthosite	C	irregular	2.647	2.474	1.094	0.708
Anorthosite	B	irregular	2.191	2.198	1.029	0.811
Anorthosite	A	irregular	1.530	1.640	0.872	0.787
Felch Marble	C	disc	0.860	0.764	0.573	0.268
Felch Marble	2	disc	0.630	0.666	0.462	0.281
Felch Marble	B	disc	0.472	0.570	0.390	0.266
Felch Marble	1	disc	0.372	0.492	0.332	0.239
Felch Marble	A	disc	0.322	0.445	0.307	0.230
Wausau quartzite	C	disc	0.700	0.803	0.488	0.283
Wausau quartzite	2	disc	0.535	0.680	0.447	0.307
Wausau quartzite	B	disc	0.397	0.545	0.414	0.267
Wausau quartzite	1	disc	0.318	0.460	0.319	0.227
Wausau quartzite	A	disc	0.166	0.362	0.327	0.211
Anorthosite	C	disc	0.856	0.864	0.543	0.267
Anorthosite	2	disc	0.662	0.760	0.472	0.302
Anorthosite	B	disc	0.556	0.634	0.463	0.278
Anorthosite	1	disc	0.420	0.548	0.421	0.280
Anorthosite	A	disc	0.339	0.463	0.309	0.230

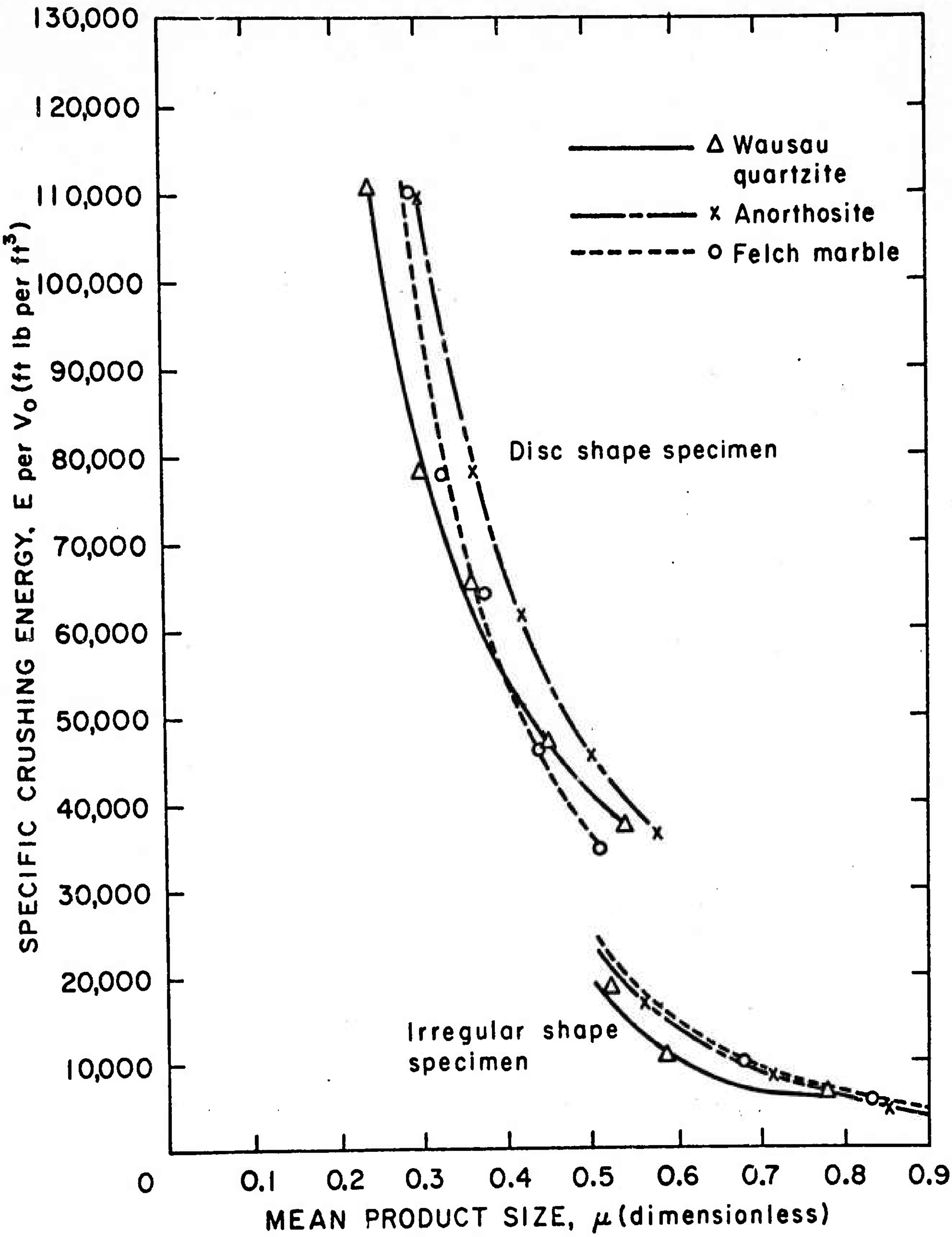

Figure 6. Power curve plots of specific crushing energy verus mean fragment size.

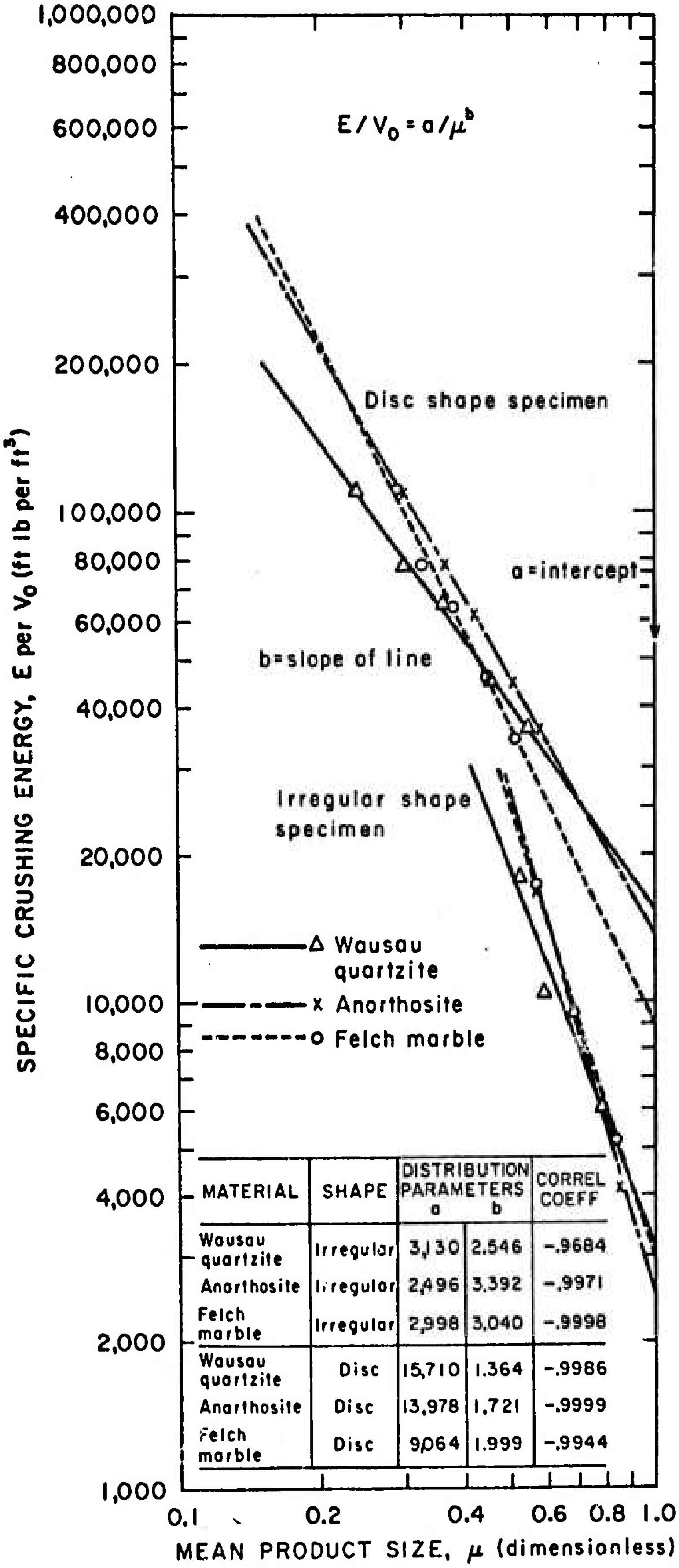

MATERIAL	SHAPE	DISTRIBUTION PARAMETERS a	b	CORREL COEFF
Wausau quartzite	Irregular	3,130	2.546	-.9684
Anorthosite	Irregular	2,496	3.392	-.9971
Felch marble	Irregular	2,998	3.040	-.9998
Wausau quartzite	Disc	15,710	1.364	-.9986
Anorthosite	Disc	13,978	1.721	-.9999
Felch marble	Disc	9,064	1.999	-.9944

Figure 7. Logarithmic plots and fitted parameters for power curves.

$X_p = X_f$). Also note that each point in figures 6 and 7 is an average for a given input energy taken from 10 points for the disc specimens and 30 points for the irregular specimens.

Another attempt at relating specific energy and mean product size was somewhat similar, but less successful. This approach consisted of fitting Charles' law (see Background) to the data points. Charles' law is given by

$$E/V_o = K\left[1/(X_2)^{n-1} - 1/(X_1)^{n-1}\right] \qquad (32)$$

where: E = specific energy (ft^3),
V_o = volume (ft^3),
X_2 = mean product sieve size (in),
X_1 = initial product sieve size (in) (3.25 in for irregular specimens and 2.00 in for disc specimens),
K,n = calculated constants related to the breaking process and the rock type.

One data analysis problem here is that there is no linearizing transformation to which a least squares fit can be made. Consequently, trial and error calculations were used to find a value of n that gave approximately constant K values for different (E/V_o, X_2) data points. The results of these calculations are summarized in table 5.

Note that the power law function and the Charles' law function are not too dissimilar, so that somewhat similar exponents can be expected. The main difference between these two functions is the subtractive term in the latter function. As pointed out in the Background section, neither of these functions is really a law, but merely a general empirical form which may or may not fit a particular breakage process and rock type.

Discussion of Results

An interpretation of the data analysis results is somewhat complicated. The rock properties shown in table 1 are not all clearly consistent with each other. It had also been postulated that in the case of the impact tests perhaps one or more of the parameters of the specific energy versus product size relationship could be correlated to one or more of these rock properties. Also it had been postulated that the parameters themselves might differentiate between rock types as to breakability. Neither postulate could be totally proved or disproved.

At the inception of this project it was planned to use several monomineralic rocks of different strengths. Initially Wausau quartzite and anorthosite were used and Felch marble was later added as this rock was expected to be weaker and softer. The eventual results of a standard

TABLE 5. - Results of fitting Charles' law to energy versus mean product size data.

Material	Shape	n	K
Wausau Quartzite	Irregular	2.5	3.53×10^4
Anorthosite	Irregular	2.8	5.03×10^4
Felch Marble	Irregular	3.1	5.10×10^4
Wausau Quartzite	Disc	2.0	4.66×10^4
Anorthosite	Disc	2.4	4.04×10^4
Felch Marble	Disc	2.7	2.66×10^4

suite of property tests (table 1) indicated a consistent trend on comparing compressive strength and hardness - Wausau quartzite was strongest and hardest, then anorthosite, and Felch marble was weakest and softest. However, tensile strength did not follow the same trend - the low value was for Wausau quartzite, which seems unlikely. Also the calculated dynamic Young's modulus turned out to be lower than the static Young's modulus for Wausau quartzite, which seems unlikely. In retrospect, perhaps the block from which the Wausau quartzite property test specimens were prepared contained more flaws than expected. Alternately the anorthosite or Felch marble properties might be inaccurate. One way to shed light on this problem would be to carry out many replications of these tests with other samples of the same material. This was not possible within the limited time, goals, and costs of this project.

The drop test experiments were performed on irregular (-3.5 + 3.0 in) specimens with the drop energy level being the only factor varied. The analysis of the distribution results of these experiments showed an apparent significant effect of the level of energy applied on the size distribution parameters.

While it was possible to make these observations based on fitting the drop test data to a negative exponential distribution, it was apparent that this distribution was not sufficiently accurate for our purposes. One reason for this is that the experimental distribution data were always bimodal rather than unimodal, as originally assumed. Subsequent analysis of the data showed that the fine material can be fitted by a separate normal distribution from the normal distribution describing the major portion of the product.

Certain inconsistencies were observed in the experimental data. Neither the mean size nor the standard deviation of the product varied in a regular manner with the applied energy. Also the slope of the fitted lines on the probability plot increased with drop height for the Wausau quartzite, but did not increase for the anorthosite (see Figs. 4a and 4b). One cause of these inconsistencies, of course, is that not all the energy goes into breakage. Another cause is the small sample sizes that resulted from lack of breakage, particularly in the case of the 25 foot drop height. Additional specimens were not run to replace those specimens that failed to break, because the impact test was going to replace the drop test.

The first impact pendulum test results were from the fragmentation sieve data analysis (Figs. 5a, 5b, 5c, 5d, 5e, and 5f). On comparing the appropriate lines on these plots, it can be seen that there was some difference in the breakability of the three rock types, but that this difference was not extremely great.

The next step was to determine whether any of the parameters of the specific energy versus product size relationship might be correlated with any of the rock properties using either the power law relationship or the Charles' law relationship. From the brief table of figure 7 for the power law and from table 5 for Charles' law, it can be seen that the only direct relationship is for the a (or K) values respectively, and then only for the disc specimens, not the irregular specimens. That is, the values of a (or K) decrease directly as compressive strength and hardness decrease, in the order Wausau quartzite, anorthosite, and Felch marble. If b (or n) were constant this ordering would imply decreasing breakability. However, b (or n) is increasing at the same time as a (or K) is decreasing. Thus no clear pattern evolves.

It appears that the b (or n) values are more important in assessing rock breakability than the a (or K) values for the higher specific energies. (Than is, the higher the line on the graph, the stronger the rock type.) As is evident from figure 7, in both the irregular and disc specimens groups of lines, some of the lines cross because the exponent b (or n) eventually "overrides" the intercept a (or K).

CONCLUSIONS AND RECOMMENDATIONS

The following conclusions can be drawn:

1. The impact pendulum rock fragmentation device proved to be a valuable tool in obtaining fragment data and energy-fragment size relationships.

2. The rock properties tested are not consistent from rock type to rock type.

3. No relationship could be established between specific energy or fragment distribution and number and size of cracks.

4. Drop test sieve distributions can be represented by composite normal distributions.

5. Impact pendulum test sieve distributions can be represented by normal distributions.

6. For the impact tests, specific crushing energy versus mean product size (for a given initial specimen or feed size) can be well represented by a power law or Charles' law. The exponents of the power law for the different rock types and shapes were generally larger than expected, compared to earlier experimental results reported in the literature.

7. The exponent of the power law appears to be the controlling factor for the higher specific energies, i.e., for higher specific energies, the larger the exponent the stronger the rock.

The following recommendations are made:

1. Some additional impact pendulum tests at slightly higher input energy (and hence higher crushing energy) levels should be run using the same rock types. Perhaps up to twice the maximum energy used in the current series could be used. (Excessive energy levels would eventually change the breakage process into some sort of grinding process, which would no longer be an approximation of a single event breakage.)

2. More extensive property determinations tests should be run, using the same three rock types.

3. Another rock type could be run if a suitably stronger and harder monomineralic rock could be found.

4. Further research and thought need to be devoted to other possible interpretations of the data analysis.

REFERENCES

1. Bergstrom, B. H., C. L. Sollenberger and W. Mitchell, Jr. Energy Aspects of Single Particle Crushing. AIME Trans. v. 223, 1962, pp. 419-422.

1A. Bergstrom, B. H. Empirical Modification of the Gaudin-Meloy Equation. AIME Trans. v. 235, 1966, p. 45.

2. Bond, F. C. The Third Theory of Comminution. AIME Trans. v. 193, May 1952, pp. 484-494.

3. Broadbent, S. R., and T. G. Calcott. Coal Breakage Processes. J. Inst. Fuel, v. 29, December 1956, pp. 524-539.

4. Charles, R. J. Energy-Size Reduction Relationship in Comminution. AIME Trans. v. 208, January 1957, pp. 80-88.

5. Epstein, B. Logarithmico-Normal Distribution in Breakage of Solids. Ind. and Eng. Chem., December 1948, pp. 2289-2291.

6. Gaudin, A. M. An Investigation of Crushing Phenomena. AIME Trans. v. 73, 1926, pp. 253-316.

7. Gaudin, A. M., and T. P. Meloy. Model and Comminution Distribution for Single Fracture. S.M.E. Trans., March 1962, AIME Trans. v. 223, 1962, pp. 40-43.

8. Gates, R. O. Kick versus Rittinger. An Experimental Investigation in Rock Crushing, Performed at Purdue University. AIME Trans. v. 52, 1916, pp. 875-909.

9. Gilvarry, J. J. Fracture of Brittle Solids I. Distribution Function for Fragment Size in Single Fracture (Theoretical). J. of Appl. Phys., v. 32, No. 3, 1961, pp. 391-399.

10. Harris, C. C. The Application of Size Distribution Equations to Multi-event Comminution Processes. AIME Trans. v. 241, September 1968, pp. 343-364.

11. Karpinski, J. M., and R. O. Tervo. Single Impact Testing of Brittle Materials. AIME Trans. v. 228, June 1964, pp. 126-130.

12. Klimpel, R. R., and L. G. Austin. The Statistical Theory of Primary Breakage Distributions for Brittle Materials. Soc. of Min. Eng. Trans. v. 232, March 1965, pp. 88-94.

13. Oka, Y. and H. Majima. Energy Requirement in Size Reduction. AIME Trans. v. 244, September 1969, pp. 249-251.

14. Rosin, P. and E. Rammler. The Laws Governing the Fineness of Powdered Coal. J. Inst. Fuel, v. 7, 1933, pp. 29-36, Discussion ibid, pp. 109-112.

15. Schuhmann, R. Jr. Principles of Comminution I - Size Distribution and Surface Calculations. AIME T. P. 1189, Min. Tech., pp. 1-11, July 1940, Discussion in T. P. 1358, 1941, pp. 2-7.

16. Walker, W. H., W. K. Lewis, W. H. McAdams, E. D. Gilliland. Principles of Chemical Engineering. McGraw-Hill Book Co., Inc., New York, 1937, Gilliland article, pp. 254-255.

APPENDIX A--BREAKAGE MATRIX ELEMENTS

Table A1 - Breakage matrix elements, b_i, (not smoothed) for irregular (-3.5 + 3.0 in) Wausau quartzite specimens.

Sieve size in	b_i - i = 1, 2, . . . , 21		
	Input energy = 164 ft-lb	Input energy = 293 ft-lb	Input energy = 455 ft-lb
-3.50 + 3.00	0.1374	0.0573	0.0679
-3.00 + 2.50	.2170	.1417	.0578
-2.50 + 2.12	.0933	.1246	.0675
-2.12 + 1.75	.1935	.1416	.1404
-1.75 + 1.50	.0816	.0879	.0910
-1.50 + 1.25	.0783	.0949	.1001
-1.25 + 1.05	.0501	.0703	.0876
-1.050 + 0.875	.0286	.0707	.0631
-0.875 + 0.742	.0172	.0329	.0416
-0.742 + 0.625	.0175	.0285	.0455
-0.625 + 0.525	.0150	.0210	.0372
-0.5250 + 0.4375	.0156	.0224	.0296
-0.4375 + 0.3750	.0074	.0154	.0221
-0.3750 + 0.3125	.0060	.0111	.0184
-0.3125 + 0.2630	.0056	.0102	.0150
-0.2630 + 0.2210	.0050	.0092	.0145
-0.2210 + 0.1850	.0034	.0059	.0103
-0.1850 + 0.1560	.0027	.0054	.0088
-0.1560 + 0.1310	.0025	.0054	.0088
-0.1310 + 0.1100	.0024	.0042	.0073
-0.1100 + 0.0930	.0019	.0037	.0063
SUM	.9820	.9643	.9408

Table A2 - Breakage matrix elements, b_i, (not smoothed) for irregular (-3.5 + 3.0 in) Anorthosite specimens.

Sieve size in	b_i - i = 1, 2, . . . , 21		
	Input energy = 164 ft-lb	Input energy = 293 ft-lb	Input energy = 455 ft-lb
-3.50 + 3.00	0.2521	0.1306	0.0343
-3.00 + 2.50	.2852	.3194	.1031
-2.50 + 2.12	.2148	.1458	.1100
-2.12 + 1.75	.1071	.1082	.2210
-1.75 + 1.50	.0258	.0751	.0984
-1.50 + 1.25	.0378	.0529	.0887
-1.25 + 1.05	.0107	.0374	.0560
-1.050 + 0.875	.0167	.0299	.0542
-0.875 + 0.742	.0065	.0141	.0325
-0.742 + 0.625	.0067	.0147	.0349
-0.625 + 0.525	.0049	.0097	.0245
-0.5250 + 0.4375	.0060	.0095	.0234
-0.4375 + 0.3750	.0026	.0076	.0151
-0.3750 + 0.3125	.0035	.0065	.0132
-0.3125 + 0.2630	.0026	.0050	.0110
-0.2630 + 0.2210	.0023	.0042	.0103
-0.2210 + 0.1850	.0016	.0030	.0072
-0.1850 + 0.1560	.0015	.0028	.0065
-0.1560 + 0.1310	.0013	.0027	.0062
-0.1310 + 0.1100	.0012	.0025	.0058
-0.1100 + 0.0930	.0010	.0020	.0048
SUM	.9919	.9836	.9611

Table A3 - Breakage matrix elements, b_i, (not smoothed) for irregular (-3.5 + 3.0 in) Felch marble specimens

Sieve size in	b_i - i = 1, 2, . . . , 21		
	Input energy = 164 ft-lb	Input energy = 293 ft-lb	Input energy = 455 ft-lb
-3.50 + 3.00	0.1770	0.1439	0.0269
-3.00 + 2.50	.1826	.1282	.0814
-2.50 + 2.12	.2589	.1411	.1384
-2.12 + 1.75	.1730	.1824	.1803
-1.75 + 1.50	.0566	.0801	.1219
-1.50 + 1.25	.0449	.0918	.1016
-1.25 + 1.05	.0295	.0408	.0755
-1.050 + 0.875	.0166	.0536	.0606
-0.875 + 0.742	.0081	.0195	.0339
-0.742 + 0.625	.0102	.0224	.0372
-0.625 + 0.525	.0102	.0167	.0213
-0.5250 + 0.4375	.0050	.0139	.0203
-0.4375 + 0.3750	.0042	.0108	.0156
-0.3750 + 0.3125	.0034	.0070	.0113
-0.3125 + 0.2630	.0031	.0063	.0102
-0.2630 + 0.2210	.0022	.0058	.0088
-0.2210 + 0.1850	.0016	.0035	.0057
-0.1850 + 0.1560	.0014	.0035	.0052
-0.1560 + 0.1310	.0012	.0033	.0049
-0.1310 + 0.1100	.0010	.0028	.0041
-0.1100 + 0.0930	.0009	.0021	.0033
SUM	.9916	.9795	.9684

Table A4 - Breakage matrix elements, b_i, (not smoothed) for disc-shaped (-2.12 + 1.75 in) Wausau quartzite specimens

Sieve size in	b_i - i = 1, 2, . . . , 18				
	Input energy = 164 ft-lb	Input energy = 223 ft-lb	Input energy = 293 ft-lb	Input energy = 365 ft-lb	Input energy = 455 ft-lb
-2.12 + 1.75	0.0000	0.0000	0.0000	0.0000	0.0000
-1.75 + 1.50	.0000	.0000	.0000	.0000	.0000
-1.50 + 1.25	.0000	.0000	.0000	.0000	.0000
-1.25 + 1.05	.0506	.0477	.0000	.0000	.0000
-1.050 + 0.875	.5110	.2609	.1312	.0373	.0265
-0.875 + 0.742	.0643	.1087	.0401	.0396	.0104
-0.742 + 0.625	.0489	.0752	.1225	.1114	.0250
-0.625 + 0.525	.0195	.0581	.1072	.0923	.0614
-0.5250 + 0.4375	.0391	.0465	.0835	.0896	.0581
-0.4375 + 0.3750	.0245	.0463	.0542	.0785	.0612
-0.3750 + 0.3125	.0217	.0422	.0474	.0697	.0656
-0.3125 + 0.2630	.0181	.0317	.0296	.0528	.0673
-0.2630 + 0.2210	.0204	.0278	.0383	.0505	.0567
-0.2210 + 0.1850	.0150	.0182	.0305	.0302	.0454
-0.1850 + 0.1560	.0194	.0194	.0241	.0297	.0422
-0.1560 + 0.1310	.0135	.0201	.0281	.0273	.0410
-0.1310 + 0.1100	.0108	.0171	.0212	.0253	.0359
-0.1100 + 0.0930	.0094	.0140	.0180	.0215	.0327
SUM	.8804	.8339	.7759	.7557	.6294

53c

Table A5 - Breakage matrix elements, b_i, (not smoothed) for disc-shaped (-2.12 + 1.75 in) anorthosite specimens

Sieve size in	b_i - i = 1, 2, . . . , 18				
	Input energy = 164 ft-lb	Input energy = 223 ft-lb	Input energy = 293 ft-lb	Input energy = 365 ft-lb	Input energy = 455 ft-lb
-2.12 + 1.75	0.0000	0.0000	0.0000	0.0000	0.0000
-1.75 + 1.50	.0000	.0000	.0000	.0000	.0000
-1.50 + 1.25	.0000	.0000	.0000	.0000	.0000
-1.25 + 1.05	.0952	.0658	.0000	.0000	.0000
-1.050 + 0.875	.6126	.4115	.2289	.1595	.0324
-0.875 + 0.742	.0318	.0777	.0971	.0487	.0516
-0.742 + 0.625	.0200	.0598	.1589	.0891	.1452
-0.625 + 0.525	.0119	.0504	.0615	.1217	.0732
-0.5250 + 0.4375	.0228	.0356	.0696	.0565	.0937
-0.4375 + 0.3750	.0165	.0277	.0393	.0666	.0648
-0.3750 + 0.3125	.0209	.0329	.0389	.0497	.0694
-0.3125 + 0.2630	.0138	.0208	.0280	.0440	.0610
-0.2630 + 0.2210	.0162	.0253	.0340	.0378	.0530
-0.2210 + 0.1850	.0127	.0155	.0215	.0267	.0333
-0.1850 + 0.1560	.0115	.0171	.0209	.0280	.0343
-0.1560 + 0.1310	.0102	.0164	.0187	.0281	.0296
-0.1310 + 0.1100	.0100	.0154	.0188	.0256	.0254
-0.1100 + 0.0930	.0086	.0124	.0154	.0209	.0223
SUM	.9147	.8843	.8515	.8029	.7892

Table A6 - Breakage matrix elements, b_i, (not smoothed) for disc-shaped (-2.12 + 1.75 in) Felch marble specimens

Sieve size in	b_i - i = 1, 2, . . . , 18				
	Input energy = 164 ft-lb	Input energy = 223 ft-lb	Input energy = 293 ft-lb	Input energy = 365 ft-lb	Input energy = 455 ft-lb
-2.12 + 1.75	0.0000	0.0000	0.0000	0.0000	0.0000
-1.75 + 1.50	.0000	.0000	.0000	.0000	.0000
-1.50 + 1.25	.0000	.0000	.0000	.0000	.0000
-1.25 + 1.05	.0000	.0000	.0000	.0000	.0000
-1.050 + 0.875	.4954	.3069	.1378	.0684	.0257
-0.875 + 0.742	.0938	.0886	.1152	.0360	.0830
-0.742 + 0.625	.0858	.1256	.1008	.1258	.0689
-0.625 + 0.525	.0411	.0737	.1106	.1205	.0882
-0.5250 + 0.4375	.0412	.0528	.0811	.0967	.0787
-0.4375 + 0.3750	.0312	.0565	.0667	.0733	.0882
-0.3750 + 0.3125	.0330	.0445	.0428	.0514	.0694
-0.3125 + 0.2630	.0218	.0297	.0437	.0510	.0697
-0.2630 + 0.2210	.0210	.0297	.0369	.0498	.0528
-0.2210 + 0.1850	.0136	.0204	.0241	.0305	.0391
-0.1850 + 0.1560	.0107	.0175	.0234	.0275	.0342
-0.1560 + 0.1310	.0125	.0158	.0226	.0274	.0323
-0.1310 + 0.1100	.0098	.0137	.0204	.0235	.0281
-0.1100 + 0.0930	.0086	.0120	.0166	.0201	.0224
SUM	.9195	.8874	.8427	.8019	.7807

APPENDIX B--MEAN PRODUCT SIZE AND SPECIFIC CRUSHING ENERGY

Table B-1. - Mean product size and specific crushing energy for material-WQ, shape-irregular, from height-C

No.	Specimen weight (lb)	Mean product size (inch)	Mean product size (dimensionless)	Standard deviation of product (inch)	Standard deviation of product (dimensionless)	Specimen output energy (ft-lb)	Crushing energy (ft-lb)	Specific crushing energy (ft-lb/ft^3)
1	1.64	1.104	0.428	0.519	0.201	67	55	5573
2	1.50	1.400	0.559	0.369	0.147	55	67	7350
3	1.66	3.240	1.249	0.164	0.063	92	30	2946
4	1.33	1.792	0.744	0.417	0.173	57	65	8041
5	1.90	3.240	1.194	0.163	0.060	69	53	4622
6	1.78	2.432	0.917	0.639	0.241	60	61	5699
7	1.42	2.121	0.861	0.677	0.275	57	64	7468
8	1.36	1.206	0.494	0.387	0.158	55	67	7953
9	1.89	2.310	0.853	0.636	0.235	55	67	5874
10	1.52	2.701	1.073	1.026	0.408	71	51	5508
11	1.79	1.522	0.572	0.592	0.222	55	67	6139
12	1.35	1.433	0.590	0.547	0.226	62	60	7351
13	0.93	2.073	0.960	0.555	0.260	67	55	9826
14	2.05	2.661	0.957	0.404	0.145	56	66	5319
15	1.36	2.532	1.045	0.544	0.224	55	67	8110
16	1.76	2.332	0.882	0.586	0.222	65	57	5364
17	1.89	3.245	1.199	0.117	0.043	96	26	2258
18	1.72	1.452	0.554	0.534	0.204	67	55	5302
19	1.43	1.573	0.637	0.761	0.308	51	71	8152
20	1.25	1.622	0.688	0.400	0.170	55	67	8894
21	1.64	2.152	0.831	0.873	0.338	58	64	6466
22	1.28	1.546	0.650	0.479	0.201	60	62	8019
23	1.62	1.265	0.492	0.428	0.167	60	62	6335
24	2.28	2.098	0.728	0.686	0.238	81	41	2985
25	1.47	1.683	0.675	0.690	0.277	60	62	6951
26	1.35	1.489	0.615	0.786	0.324	79	43	5204
27	1.38	1.489	0.610	0.487	0.200	67	55	6606
28	2.10	1.917	0.684	0.437	0.156	71	51	3981
29	1.79	2.497	0.940	0.404	0.152	90	32	2943
30	1.49	1.780	0.712	0.625	0.250	62	60	6684
Average	1.60	1.997	0.780	0.531	0.209	65	57	6131
Composite		2.052	0.799	0.835	0.326			

Table B-2 - Mean product size and specific crushing energy for material-WQ, shape-irregular, from height-B.

No.	Specimen weight (lb)	Mean product size (inch)	Mean product size (dimensionless)	Standard deviation of product (inch)	Standard deviation of product (dimensionless)	Specimen output energy (ft-lb)	Crushing energy (ft-lb)	Specific crushing energy (ft-lb/ft^3)
1	1.94	1.350	0.494	0.452	0.165	119	102	8623
2	1.71	2.285	0.873	0.623	0.238	109	112	10753
3	1.52	0.885	0.352	0.371	0.147	123	97	10587
4	1.52	1.520	0.603	0.580	0.230	128	92	9971
5	0.99	0.925	0.423	0.525	0.240	123	97	16171
6	1.49	1.026	0.410	0.401	0.160	113	107	11815
7	1.69	1.719	0.659	0.613	0.235	116	104	10138
8	1.79	1.659	0.625	0.657	0.247	114	107	9841
9	1.65	2.504	0.967	0.610	0.236	111	109	10878
10	1.70	1.534	0.587	0.540	0.206	109	112	10796
11	1.32	0.899	0.374	0.363	0.151	113	107	13291
12	2.19	2.115	0.744	0.627	0.220	119	101	7638
13	1.82	1.429	0.535	0.566	0.212	101	119	10777
14	1.86	1.448	0.537	0.799	0.296	145	75	6619
15	2.25	1.834	0.639	0.861	0.300	103	117	8602
16	3.43	3.035	0.919	0.661	0.200	136	84	4063
17	2.16	2.004	0.708	0.532	0.188	116	104	7936
18	1.00	1.028	0.363	0.444	0.202	105	115	18856
19	1.76	1.479	0.560	0.583	0.221	108	112	10552
20	1.30	1.493	0.624	0.797	0.333	106	114	14404
21	1.38	0.911	0.374	0.373	0.153	118	102	12135
22	1.51	1.313	0.523	0.516	0.205	147	73	7969
23	1.38	1.198	0.491	0.413	0.169	111	109	13020
24	1.98	2.245	0.816	0.709	0.258	95	125	10398
25	2.13	1.959	0.695	0.558	0.198	119	101	7846
26	1.02	0.861	0.390	0.353	0.160	113	107	17237
27	1.69	1.027	0.394	0.378	0.145	105	116	11277
28	2.78	2.567	0.833	0.571	0.185	126	94	5602
29	2.13	1.608	0.570	0.625	0.222	118	102	7921
30	2.22	1.352	0.473	0.685	0.240	102	119	8815
Average	1.78	1.574	0.585	0.560	0.212	116	104	10484
Composite		1.713	0.639	0.838	0.316			

Table B-3 - Mean product size and specific crushing energy for material-WQ, shape-irregular, from height-A.

No.	Specimen weight (lb)	Mean product size (inch)	Mean product size (dimensionless)	Standard deviation of product (inch)	Standard deviation of product (dimensionless)	Specimen output energy (ft-lb)	Crushing energy (ft-lb)	Specific crushing energy (ft-lb/ft^3)
1	2.02	1.585	0.573	0.673	0.243	148	206	16899
2	1.50	0.821	0.327	0.455	0.181	171	184	20250
3	1.78	0.735	0.276	0.403	0.152	156	199	18390
4	1.61	2.332	0.909	0.786	0.306	156	199	20388
5	2.38	1.769	0.605	0.657	0.224	176	178	12366
6	1.60	0.785	0.306	0.310	0.121	149	206	21165
7	1.84	1.985	0.740	0.487	0.181	160	195	17488
8	1.59	0.872	0.341	0.481	0.188	219	136	14073
9	1.80	1.011	0.379	0.455	0.171	144	211	19353
10	1.36	1.185	0.488	0.475	0.195	151	204	24632
11	2.13	1.814	0.644	0.396	0.140	168	187	14436
12	2.02	1.126	0.406	0.626	0.226	160	195	15882
13	1.50	0.946	0.377	0.409	0.163	180	175	19209
14	1.81	1.353	0.507	0.711	0.266	160	195	17772
15	1.04	1.052	0.474	0.532	0.239	183	172	27096
16	1.43	0.938	0.380	0.388	0.157	148	207	23806
17	1.71	0.987	0.377	0.612	0.233	155	200	19264
18	1.37	1.212	0.414	0.521	0.214	156	199	23993
19	2.38	2.715	0.930	0.900	0.308	187	168	11669
20	1.29	1.256	0.527	0.619	0.259	171	184	23500
21	1.61	1.273	0.496	0.545	0.212	214	140	14383
22	1.62	1.073	0.417	0.418	0.162	160	195	19815
23	1.26	0.599	0.253	0.351	0.148	222	132	17269
24	1.71	2.063	0.787	0.766	0.292	166	189	18176
25	2.19	1.194	0.420	0.600	0.211	148	206	15587
26	2.08	1.114	0.399	0.562	0.201	163	192	15245
27	2.39	1.954	0.668	0.826	0.282	155	200	13802
28	2.01	1.466	0.531	0.666	0.241	168	187	15366
29	1.94	3.149	1.153	0.475	0.174	191	164	13906
30	1.58	1.429	0.561	0.581	0.228	163	192	20054
Average	1.75	1.393	0.522	0.556	0.211	168	187	18174
Composite		1.476	0.554	0.852	0.323			

Table B-4 - Mean product size and specific crushing energy for material-AN, shape-irregular, from height-C.

No.	Specimen weight (lb)	Mean product size (inch)	Mean product size (dimensionless)	Standard deviation of product (inch)	Standard deviation of product (dimensionless)	Specimen output energy (ft-lb)	Crushing energy (ft-lb)	Specific crushing energy (ft-lb/ft^3)
1	2.76	2.892	0.947	0.603	0.197	60	62	3770
2	2.52	2.988	1.009	0.434	0.146	81	40	2698
3	1.64	2.499	0.972	0.431	0.168	73	49	4982
4	1.74	2.086	0.797	0.473	0.180	71	51	4969
5	1.85	1.984	0.741	0.402	0.150	84	38	3490
6	2.16	2.351	0.836	0.581	0.206	71	51	4001
7	1.73	2.227	0.852	0.384	0.147	68	54	5245
8	1.97	3.178	1.165	0.426	0.156	60	62	5299
9	2.08	3.235	1.164	0.207	0.074	65	57	4607
10	2.20	1.936	0.684	0.553	0.195	91	31	2379
11	2.24	2.130	0.746	0.633	0.222	78	44	3305
12	2.18	2.251	0.798	0.569	0.201	65	57	4404
13	3.00	2.677	0.853	0.358	0.114	89	32	1820
14	2.92	2.639	0.849	0.417	0.134	84	38	2203
15	1.96	2.258	0.829	0.690	0.253	58	64	5536
16	1.55	2.400	0.952	0.678	0.269	77	45	4911
17	1.84	2.388	0.895	0.773	0.290	75	47	4327
18	1.63	1.670	0.652	0.523	0.204	61	61	6290
19	1.45	3.241	1.314	0.163	0.066	69	53	6178
20	2.68	2.720	0.899	0.740	0.244	58	64	4030
21	2.62	2.381	0.794	0.618	0.206	79	43	2774
22	2.62	2.825	0.942	0.714	0.238	61	61	3894
23	4.80	3.234	0.882	0.203	0.055	50	72	2508
24	2.41	2.222	0.762	0.639	0.219	62	60	4156
25	2.87	2.336	0.756	0.476	0.154	62	60	3526
26	2.40	1.828	0.627	0.566	0.194	66	56	3954
27	1.50	1.662	0.652	0.483	0.190	74	47	4989
28	2.03	2.591	0.940	0.231	0.084	73	49	4087
29	1.87	1.793	0.668	0.545	0.203	78	44	3948
30	1.38	1.385	0.571	0.468	0.193	72	50	6107
Average	2.22	2.400	0.852	0.499	0.178	70	52	4146
Composite		2.474	0.869	0.708	0.249			

Table B-5. -Mean product size and specific crushing energy for material-AN, shape-irregular, from height-B.

No.	Specimen weight (lb)	Mean product size (inch)	Mean product size (dimensionless)	Standard deviation of product (inch)	Standard deviation of product (dimensionless)	Specimen output energy (ft-lb)	Crushing energy (ft-lb)	Specific crushing energy (ft-lb/ft³)
1	2.43	2.285	0.781	0.716	0.245	125	95	6612
2	2.16	1.995	0.709	0.853	0.303	120	101	7823
3	2.35	2.712	0.937	0.297	0.102	120	101	7188
4	1.20	1.290	0.556	0.560	0.242	112	108	15146
5	1.90	2.562	0.950	0.591	0.219	122	98	8659
6	1.73	1.210	0.463	0.462	0.177	122	98	9550
7	1.75	1.900	0.724	0.502	0.191	112	108	10419
8	1.22	0.921	0.390	0.380	0.163	124	96	13148
9	1.79	1.541	0.584	0.528	0.200	105	116	10873
10	2.40	2.181	0.748	0.735	0.252	115	106	7388
11	4.39	3.241	0.910	0.158	0.044	149	71	2725
12	2.61	2.047	0.683	0.655	0.219	102	119	7637
13	2.28	2.579	0.901	0.559	0.195	134	86	6322
14	2.89	2.319	0.748	0.629	0.203	133	87	5079
15	2.88	2.341	0.756	0.626	0.202	136	84	4890
16	2.72	2.137	0.704	0.683	0.225	98	122	7575
17	1.58	1.579	0.623	0.515	0.203	121	99	10545
18	2.04	2.035	0.737	0.549	0.199	111	109	8977
19	2.48	2.933	0.995	0.816	0.277	113	107	7279
20	1.72	2.008	0.766	0.605	0.232	98	122	11918
21	2.94	1.638	0.525	0.673	0.216	108	112	6413
22	1.28	1.650	0.695	0.702	0.297	124	96	12542
23	1.68	1.452	0.560	0.364	0.140	140	80	8019
24	1.79	1.509	0.570	0.536	0.203	109	111	10364
25	1.60	1.270	0.499	0.721	0.283	136	84	8846
26	4.08	2.664	0.766	0.411	0.118	103	117	4842
27	3.58	2.205	0.662	0.704	0.211	140	80	3750
28	2.46	2.180	0.742	0.693	0.236	99	121	8259
29	2.36	2.056	0.710	0.431	0.149	106	114	8112
30	2.53	3.230	1.089	0.237	0.080	140	80	5315
Average	2.29	2.056	0.716	0.563	0.201	119	101	8207
Composite		2.198	0.763	0.811	0.283			

Table B-6. - Mean product size and specific crushing energy for material-AN, shape-irregular, from height-A.

No.	Specimen weight (lb)	Mean product size (inch)	Mean product size (dimensionless)	Standard deviation of product (inch)	Standard deviation of product (dimensionless)	Specimen output energy (ft-lb)	Crushing energy (ft-lb)	Specific crushing energy (ft-lb/ft^3)
1	2.28	1.596	0.557	0.561	0.196	151	204	15037
2	2.82	1.970	0.641	0.870	0.283	155	199	11885
3	1.75	1.982	0.756	0.900	0.343	163	192	18470
4	2.26	1.202	0.421	0.529	0.185	162	193	14351
5	2.51	2.860	0.967	0.911	0.308	166	189	12646
6	2.52	2.136	0.722	0.712	0.240	162	193	12868
7	2.03	1.895	0.687	0.544	0.197	184	171	14167
8	1.17	0.867	0.378	0.382	0.167	172	183	26352
9	1.59	0.965	0.379	0.523	0.206	179	176	18513
10	2.51	2.062	0.697	0.901	0.305	141	214	14334
11	2.18	1.147	0.406	0.562	0.199	202	153	11770
12	2.01	1.274	0.464	0.482	0.176	175	180	15043
13	1.49	1.460	0.587	0.580	0.233	183	171	19263
14	1.63	1.168	0.456	0.474	0.185	143	212	21910
15	2.15	1.150	0.409	0.589	0.209	136	219	17055
16	2.83	1.768	0.575	0.653	0.212	145	210	12500
17	1.58	1.262	0.498	0.464	0.183	172	183	19464
18	2.64	1.910	0.635	0.584	0.194	163	192	12225
19	2.02	1.894	0.689	0.580	0.211	184	171	14242
20	1.58	1.139	0.449	0.523	0.206	200	155	16471
21	1.19	1.122	0.485	0.608	0.263	167	188	26421
22	1.33	0.810	0.338	0.374	0.156	157	198	25069
23	2.13	1.179	0.421	0.569	0.203	135	219	17311
24	1.46	1.532	0.620	0.613	0.248	130	225	25373
25	1.75	1.338	0.510	0.575	0.219	163	192	18423
26	2.52	1.825	0.616	0.587	0.198	141	214	14250
27	2.00	1.360	0.496	0.578	0.211	157	198	16637
28	1.80	1.663	0.627	0.629	0.237	167	188	17495
29	1.83	1.777	0.667	0.450	0.169	172	183	16747
30	2.81	2.266	0.739	0.643	0.209	148	207	12419
Average	2.01	1.553	0.563	0.598	0.218	162	192	16974
Composite		1.640	0.595	0.787	0.286			

Table B-7. - Mean product size and specific crushing energy for material-FM, shape-irregular, from height-C.

No.	Specimen weight (lb)	Mean product size (inch)	Mean product size (dimensionless)	Standard deviation of product (inch)	Standard deviation of product (dimensionless)	Specimen output energy (ft-lb)	Crushing energy (ft-lb)	Specific crushing energy (ft-lb/ft^3)
1	1.95	1.444	0.544	0.500	0.188	50	72	6715
2	2.10	2.343	0.861	0.655	0.241	45	77	6585
3	1.86	1.857	0.710	0.506	0.193	59	63	6127
4	1.57	1.889	0.765	0.587	0.237	56	66	7601
5	2.40	3.247	1.142	0.085	0.030	71	51	3864
6	2.04	3.128	1.162	0.506	0.188	65	56	5005
7	1.87	1.951	0.746	0.614	0.235	58	64	6222
8	1.79	2.181	0.845	0.829	0.321	70	52	5247
9	1.46	2.108	0.876	0.934	0.388	66	56	6932
10	1.97	3.061	1.149	0.628	0.235	65	57	5224
11	1.73	1.618	0.635	0.386	0.151	70	52	5431
12	1.73	2.089	0.819	0.811	0.318	70	52	5433
13	2.94	2.774	0.912	0.715	0.235	62	59	3656
14	2.48	2.092	0.727	0.415	0.144	60	62	4520
15	2.12	2.013	0.738	0.440	0.161	46	76	6477
16	2.21	1.985	0.718	0.407	0.147	60	62	5066
17	1.74	2.177	0.851	0.230	0.089	74	48	4976
18	2.67	2.078	0.705	0.539	0.183	62	60	4025
19	2.44	2.107	0.737	0.475	0.166	53	69	5110
20	2.50	2.202	0.764	0.625	0.217	84	38	2775
21	2.45	2.637	0.920	0.438	0.153	58	64	4738
22	2.07	1.949	0.720	0.431	0.159	58	64	5621
23	2.45	2.246	0.784	0.614	0.214	58	64	4736
24	2.21	3.248	1.174	0.075	0.027	88	34	2781
25	1.73	1.940	0.761	0.404	0.158	77	45	4742
26	1.69	1.986	0.784	0.361	0.142	69	53	5616
27	1.34	2.897	1.236	0.889	0.379	65	57	7686
28	2.47	2.145	0.747	0.778	0.271	62	60	4361
29	1.96	1.788	0.672	0.305	0.114	70	52	4792
30	1.82	1.909	0.736	0.496	0.191	58	64	6397
Average	2.06	2.236	0.831	0.523	0.196	64	58	5282
Composite		2.264	0.836	0.724	0.268			

Table B-8. - Mean product size and specific crushing energy for material-FM, shape-irregular, from height-B.

No.	Specimen weight (lb)	Mean product size (inch)	Mean product size (dimensionless)	Standard deviation of product (inch)	Standard deviation of product (dimensionless)	Specimen output energy (ft-lb)	Crushing energy (ft-lb)	Specific crushing energy (ft-lb/ft^3)
1	1.39	0.964	0.406	0.387	0.163	135	85	11012
2	1.63	1.559	0.623	0.469	0.187	123	97	10749
3	1.40	1.233	0.519	0.512	0.215	104	116	15026
4	2.99	2.982	0.975	0.435	0.142	123	97	5860
5	1.97	1.266	0.475	0.536	0.201	101	119	10858
6	1.61	2.859	1.148	0.786	0.315	119	102	11383
7	2.46	2.462	0.858	0.607	0.211	112	108	7944
8	1.99	1.978	0.741	0.500	0.187	114	107	9675
9	1.67	1.211	0.480	0.415	0.164	127	93	10030
10	2.14	1.647	0.602	0.673	0.245	127	93	7831
11	1.32	1.414	0.607	0.484	0.207	134	86	11743
12	3.17	2.062	0.661	0.618	0.198	107	113	6436
13	1.29	1.138	0.492	0.554	0.239	104	116	16216
14	2.32	1.548	0.550	0.517	0.184	116	104	8093
15	1.83	1.339	0.515	0.595	0.229	116	104	10276
16	2.67	1.926	0.654	0.603	0.204	130	90	6095
17	2.54	2.880	0.994	0.575	0.198	119	101	7201
18	1.90	2.000	0.760	0.451	0.171	123	97	9247
19	2.00	1.540	0.576	0.536	0.200	104	116	10520
20	2.35	1.981	0.701	0.361	0.128	105	115	8885
21	1.77	1.388	0.540	0.493	0.192	124	96	9859
22	2.54	2.343	0.809	0.674	0.233	112	108	7701
23	2.11	2.802	1.029	0.880	0.323	134	86	7338
24	2.59	3.238	1.110	0.182	0.062	130	90	6280
25	1.94	1.741	0.657	0.654	0.247	127	93	8640
26	2.58	1.864	0.639	0.798	0.274	105	115	8078
27	1.23	1.223	0.537	0.581	0.255	123	97	14320
28	2.44	2.225	0.778	0.722	0.252	135	86	6328
29	1.63	1.384	0.553	0.525	0.210	119	102	11232
30	1.42	0.947	0.396	0.380	0.159	130	90	11484
Average	2.03	1.838	0.679	0.550	0.207	119	101	9545
Composite		1.958	0.726	0.851	0.316			

Table B-9. - Mean product size and specific crushing energy for material-FM, shape-irregular, from height-A.

No.	Specimen weight (lb)	Mean product size (inch)	Mean product size (dimensionless)	Standard deviation of product (inch)	Standard deviation of product (dimensionless)	Specimen output energy (ft-lb)	Crushing energy (ft-lb)	Specific crushing energy ($ft\text{-}lb/ft^3$)
1	2.01	1.496	0.558	0.761	0.284	194	160	14416
2	2.10	1.917	0.704	0.960	0.353	171	184	15778
3	1.63	1.016	0.406	0.433	0.173	162	193	21344
4	2.98	1.371	0.448	0.514	0.168	174	180	10930
5	1.79	1.688	0.654	0.637	0.247	155	200	20156
6	2.85	2.335	0.776	0.658	0.218	190	165	10437
7	1.47	0.895	0.370	0.329	0.136	187	168	20576
8	1.67	0.916	0.363	0.411	0.163	167	188	20323
9	1.54	1.254	0.511	0.522	0.213	178	177	20707
10	2.86	1.094	0.363	0.429	0.142	166	189	11931
11	2.01	1.346	0.501	0.478	0.178	146	208	18683
12	2.23	1.866	0.672	0.578	0.208	171	184	14869
13	1.86	1.609	0.616	0.460	0.176	158	197	19107
14	2.11	1.862	0.683	0.564	0.207	180	174	14901
15	1.08	0.996	0.456	0.495	0.227	180	175	29153
16	1.76	1.685	0.657	0.666	0.259	174	181	18494
17	1.31	1.041	0.448	0.528	0.227	186	168	23247
18	1.97	1.332	0.500	0.525	0.197	196	158	14482
19	1.56	1.847	0.749	0.569	0.231	197	157	18175
20	3.46	2.385	0.742	0.643	0.200	156	199	10414
21	2.55	1.287	0.443	0.561	0.193	169	186	13126
22	1.45	1.264	0.526	0.395	0.164	185	169	21114
23	1.71	1.252	0.493	0.579	0.228	171	184	19454
24	2.45	2.704	0.945	0.876	0.306	171	184	13560
25	2.46	1.655	0.577	0.475	0.166	202	153	11224
26	1.96	1.913	0.720	0.492	0.185	173	182	16746
27	1.31	1.041	0.447	0.409	0.176	159	196	26971
28	3.19	1.750	0.560	0.723	0.231	163	191	10856
29	2.72	1.661	0.560	0.560	0.189	165	190	12583
30	2.02	1.424	0.530	0.527	0.196	156	199	17786
Average	2.07	1.530	0.566	0.559	0.208	174	181	17051
Composite		1.612	0.593	0.745	0.275			

Table B-10. -Mean product size and specific crushing energy for material-WQ, shape-cylinder, from height-C.

No.	Specimen weight (lb)	Mean product size (inch)	Mean product size (dimensionless)	Standard deviation of product (inch)	Standard deviation of product (dimensionless)	Specimen output energy (ft-lb)	Crushing energy (ft-lb)	Specific crushing energy (ft-lb/ft^3)
1	0.31	0.750	0.506	0.291	0.196	56	66	35271
2	0.30	0.832	0.566	0.256	0.174	60	62	33449
3	0.30	0.741	0.501	0.271	0.183	52	70	37568
4	0.30	0.768	0.520	0.278	0.189	50	72	38785
5	0.30	0.714	0.487	0.283	0.193	52	70	38473
6	0.30	0.721	0.489	0.312	0.212	53	69	37065
7	0.31	0.801	0.541	0.260	0.175	48	74	39184
8	0.30	1.021	0.692	0.205	0.139	53	69	36932
9	0.30	0.865	0.588	0.211	0.143	59	63	34447
10	0.30	0.733	0.500	0.305	0.208	56	66	36327
Average	0.30	0.794	0.539	0.267	0.181	54	68	36750
Composite		0.803	0.541	0.283	0.192			

Table B-11. - Mean product size and specific crushing energy for material-WQ, shape-cylinder, from height-2.

No.	Specimen weight (lb)	Mean product size (inch)	Mean product size (dimensionless)	Standard deviation of product (inch)	Standard deviation of product (dimensionless)	Specimen output energy (ft-lb)	Crushing energy (ft-lb)	Specific crushing energy (ft-lb/ft^3)
1	0.31	0.778	0.524	0.305	0.205	69	91	48013
2	0.31	0.797	0.533	0.277	0.185	72	88	45491
3	0.31	0.544	0.366	0.222	0.150	70	90	47230
4	0.31	0.525	0.352	0.212	0.142	77	83	43327
5	0.31	0.724	0.487	0.273	0.183	77	83	43784
6	0.31	0.497	0.332	0.219	0.147	75	85	43905
7	0.31	0.569	0.384	0.326	0.220	72	88	46620
8	0.31	0.853	0.574	0.325	0.218	72	88	45429
9	0.32	0.651	0.433	0.329	0.219	70	90	45689
10	0.31	0.767	0.515	0.290	0.194	69	91	47446
Average	0.31	0.671	0.450	0.278	0.186	73	87	45694
Composite		0.680	0.453	0.307	0.206			

Table B-12 - Mean product size and specific crushing energy for material-WQ, shape-cylinder, from height-B.

No.	Specimen weight (lb)	Mean product size (inch)	Mean product size (dimensionless)	Standard deviation of product (inch)	Standard deviation of product (dimensionless)	Specimen output energy (ft-lb)	Crushing energy (ft-lb)	Specific crushing energy (ft-lb/ft^3)
1	0.30	0.520	0.352	0.216	0.146	100	121	64789
2	0.30	0.541	0.366	0.274	0.185	103	117	62838
3	0.30	0.458	0.310	0.198	0.134	94	126	67715
4	0.30	0.686	0.465	0.296	0.200	100	121	64789
5	0.28	0.369	0.256	0.175	0.121	109	111	63979
6	0.30	0.417	0.283	0.190	0.129	96	124	67335
7	0.31	0.633	0.427	0.288	0.195	98	122	65106
8	0.31	0.738	0.496	0.275	0.185	94	126	66335
9	0.31	0.526	0.355	0.236	0.159	100	120	63687
10	0.30	0.437	0.297	0.209	0.142	100	121	65398
Average	0.30	0.532	0.361	0.236	0.160	99	121	65197
Composite		0.545	0.366	0.267	0.181			

Table B-13. - Mean product size and specific crushing energy for material-WQ, shape-cylinder, from height-1.

No.	Specimen weight (lb)	Mean product size (inch)	Mean product size (dimensionless)	Standard deviation of product (inch)	Standard deviation of product (dimensionless)	Specimen output energy (ft-lb)	Crushing energy (ft-lb)	Specific crushing energy (ft-lb/ft^3)
1	0.31	0.531	0.358	0.358	0.184	117	154	81545
2	0.31	0.406	0.273	0.201	0.135	125	146	76754
3	0.31	0.437	0.293	0.187	0.125	125	146	75956
4	0.32	0.419	0.280	0.218	0.146	122	150	76953
5	0.31	0.383	0.257	0.223	0.150	118	153	80699
6	0.31	0.620	0.418	0.278	0.187	118	153	81385
7	0.31	0.352	0.235	0.152	0.102	125	146	75746
8	0.31	0.548	0.370	0.263	0.177	122	150	79516
9	0.31	0.335	0.226	0.147	0.099	128	144	75799
10	0.30	0.468	0.316	0.188	0.127	122	150	80255
Average	0.31	0.450	0.303	0.204	0.137	122	149	78461
Composite		0.460	0.306	0.227	0.152			

Table B-14 - Mean product size and specific crushing energy for material-WQ, shape-cylinder, from height-A.

No.	Specimen weight (lb)	Mean product size (inch)	Mean product size (dimensionless)	Standard deviation of product (inch)	Standard deviation of product (dimensionless)	Specimen output energy (ft-lb)	Crushing energy (ft-lb)	Specific crushing energy (ft-lb/ft^3)
1	0.31	0.268	0.181	0.136	0.092	151	204	108597
2	0.30	0.418	0.283	0.291	0.197	154	201	108446
3	0.30	0.316	0.214	0.162	0.110	146	209	112400
4	0.30	0.309	0.209	0.151	0.102	145	210	112744
5	0.30	0.303	0.205	0.157	0.106	151	204	109373
6	0.30	0.436	0.296	0.310	0.210	143	212	113832
7	0.30	0.344	0.233	0.159	0.107	154	201	108057
8	0.31	0.370	0.249	0.172	0.115	139	215	112674
9	0.31	0.416	0.280	0.233	0.157	154	201	106456
10	0.30	0.368	0.250	0.180	0.122	148	207	112595
Average	0.30	0.355	0.240	0.195	0.132	148	206	110517
Composite		0.362	0.241	0.211	0.142			

Table B-15 -- Mean product size and specific crushing energy for material-AN, shape-cylinder, from height-C.

No.	Specimen weight (lb)	Mean product size (inch)	Mean product size (dimensionless)	Standard deviation of product (inch)	Standard deviation of product (dimensionless)	Specimen output energy (ft-lb)	Crushing energy (ft-lb)	Specific crushing energy (ft-lb/ft^3)
1	0.31	0.870	0.587	0.229	0.155	47	75	39627
2	0.32	0.796	0.533	0.248	0.166	52	70	36263
3	0.32	0.813	0.546	0.252	0.169	56	66	34375
4	0.32	1.024	0.686	0.196	0.131	56	66	34489
5	0.32	0.943	0.632	0.300	0.201	53	69	35775
6	0.32	0.780	0.523	0.296	0.198	56	66	34654
7	0.32	0.848	0.569	0.252	0.169	52	70	36628
8	0.32	0.837	0.559	0.267	0.178	52	70	36184
9	0.32	0.857	0.572	0.253	0.169	52	70	35872
10	0.32	0.811	0.545	0.271	0.182	51	71	37563
Average	0.32	0.858	0.575	0.256	0.172	53	69	36143
Composite		0.864	0.576	0.267	0.179			

Table B-16 - Mean product size and specific crushing energy for material-AN, shape-cylinder, from height-2.

No.	Specimen weight (lb)	Mean product size (inch)	Mean product size (dimensionless)	Standard deviation of product (inch)	Standard deviation of product (dimensionless)	Specimen output energy (ft-lb)	Crushing energy (ft-lb)	Specific crushing energy (ft-lb/ft^3)
1	0.31	0.776	0.522	0.296	0.199	71	89	47113
2	0.32	0.698	0.469	0.295	0.198	71	89	46758
3	0.32	0.680	0.455	0.279	0.187	69	91	47218
4	0.32	0.646	0.432	0.272	0.182	77	83	42944
5	0.31	0.940	0.633	0.275	0.185	75	85	44666
6	0.32	0.787	0.527	0.271	0.181	75	85	44088
7	0.32	0.796	0.534	0.294	0.197	69	91	47314
8	0.32	0.914	0.614	0.291	0.196	77	83	43681
9	0.32	0.665	0.445	0.289	0.193	71	89	46188
10	0.32	0.628	0.422	0.275	0.184	79	81	42331
Average	0.32	0.753	0.505	0.284	0.190	73	87	45230
Composite		0.760	0.506	0.302	0.203			

Table B-17 - Mean product size and specific crushing energy for material-AN, shape-cylinder, from height-B.

No.	Specimen weight (lb)	Mean product size (inch)	Mean product size (dimensionless)	Standard deviation of product (inch)	Standard deviation of product (dimensionless)	Specimen output energy (ft-lb)	Crushing energy (ft-lb)	Specific crushing energy (ft-lb/ft^3)
1	0.32	0.590	0.395	0.246	0.165	98	122	63525
2	0.32	0.591	0.394	0.227	0.151	100	120	61233
3	0.32	0.704	0.471	0.278	0.185	95	125	64674
4	0.32	0.644	0.432	0.277	0.186	113	107	55859
5	0.32	0.615	0.411	0.271	0.181	109	111	57412
6	0.32	0.580	0.389	0.298	0.200	93	127	66396
7	0.31	0.534	0.360	0.212	0.143	108	112	59112
8	0 [illegible]	0.723	0.483	0.304	0.203	97	123	63321
9	[illegible].32	0.690	0.463	0.313	0.210	103	117	61100
10	0.32	0.619	0.416	0.278	0.187	95	125	65606
Average	0.32	0.629	0.421	0.270	0.181	101	119	61824
Composite		0.634	0.422	0.278	0.186			

Table B-18 - Mean product size and specific crushing energy for material-AN, shape-cylinder, from height-1.

No.	Specimen weight (lb)	Mean product size (inch)	Mean product size (dimensionless)	Standard deviation of product (inch)	Standard deviation of product (dimensionless)	Specimen output energy (ft-lb)	Crushing energy (ft-lb)	Specific crushing energy (ft-lb/ft^3)
1	0.32	0.630	0.423	0.317	0.213	120	151	79068
2	0.31	0.513	0.348	0.261	0.177	118	153	82852
3	0.32	0.674	0.452	0.303	0.203	123	148	77548
4	0.32	0.384	0.258	0.160	0.107	120	151	78906
5	0.32	0.538	0.362	0.315	0.212	114	158	82839
6	0.31	0.559	0.376	0.267	0.180	123	148	78202
7	0.32	0.572	0.382	0.291	0.195	126	145	75147
8	0.31	0.527	0.355	0.194	0.131	138	134	70619
9	0.32	0.483	0.323	0.284	0.190	123	148	76668
10	0.31	0.541	0.364	0.263	0.177	118	153	80624
Average	0.32	0.542	0.364	0.266	0.178	122	149	78231
Composite		0.548	0.365	0.280	0.188			

Table B-19 - Mean product size and specific crushing energy for material-AN, shape-cylinder, from height-A.

No.	Specimen weight (lb)	Mean product size (inch)	Mean product size (dimensionless)	Standard deviation of product (inch)	Standard deviation of product (dimensionless)	Specimen output energy (ft-lb)	Crushing energy (ft-lb)	Specific crushing energy (ft-lb/ft^3)
1	0.32	0.487	0.326	0.188	0.126	13[illegible]	217	113004
2	0.31	0.426	0.288	0.218	0.147	139	215	114946
3	0.32	0.346	0.232	0.175	0.117	140	214	112028
4	0.32	0.532	0.356	0.215	0.143	139	215	111442
5	0.32	0.459	0.307	0.275	0.184	139	215	111594
6	0.32	0.664	0.443	0.249	0.166	167	187	96172
7	0.32	0.387	0.260	0.159	0.107	152	203	106852
8	0.32	0.430	0.288	0.197	0.132	143	212	110121
9	0.32	0.422	0.282	0.224	0.150	134	221	114427
10	0.32	0.368	0.246	0.182	0.121	147	208	108020
Average	0.32	0.452	0.303	0.208	0.139	144	211	109861
Composite		0.463	0.307	0.230	0.154			

Table B-20 - Mean product size and specific crushing energy for material-FM, shape-cylinder, from height-C.

No.	Specimen weight (lb)	Mean product size (inch)	Mean product size (dimensionless)	Standard deviation of product (inch)	Standard deviation of product (dimensionless)	Specimen output energy (ft-lb)	Crushing energy (ft-lb)	Specific crushing energy (ft-lb/ft^3)
1	0.33	0.795	0.541	0.282	0.192	62	60	32575
2	0.34	0.690	0.464	0.287	0.193	61	61	32232
3	0.35	0.852	0.567	0.232	0.161	65	57	29285
4	0.33	0.691	0.470	0.253	0.172	54	67	36666
5	0.34	0.681	0.457	0.250	0.168	54	67	35355
6	0.33	0.878	0.594	0.211	0.142	62	60	32043
7	0.33	0.722	0.488	0.260	0.176	55	67	35833
8	0.33	0.780	0.528	0.253	0.171	54	68	36588
9	0.33	0.721	0.487	0.278	0.188	52	70	37351
10	0.33	0.773	0.525	0.271	0.184	51	71	38500
Average	0.33	0.758	0.512	0.259	0.175	57	65	34643
Composite		0.764	0.513	0.268	0.181			

Table B-21 - Mean product size and specific crushing energy for material-FM, shape-cylinder, from height-2.

No.	Specimen weight (lb)	Mean product size (inch)	Mean product size (dimensionless)	Standard deviation of product (inch)	Standard deviation of product (dimensionless)	Specimen output energy (ft-lb)	Crushing energy (ft-lb)	Specific crushing energy (ft-lb/ft^3)
1	0.34	0.714	0.479	0.297	0.199	71	89	46446
2	0.34	0.529	0.356	0.227	0.153	75	85	44885
3	0.33	0.649	0.441	0.292	0.198	75	85	46040
4	0.34	0.702	0.474	0.306	0.206	69	91	48494
5	0.34	0.595	0.400	0.244	0.164	69	91	47874
6	0.34	0.795	0.532	0.264	0.177	78	82	42738
7	0.36	0.867	0.573	0.237	0.156	74	86	43069
8	0.34	0.470	0.316	0.171	0.115	69	91	47644
9	0.33	0.595	0.403	0.262	0.177	71	89	47752
10	0.33	0.651	0.441	0.232	0.157	69	91	49021
Average	0.34	0.657	0.441	0.253	0.170	72	88	46396
Composite		0.666	0.444	0.281	0.189			

Table B-22 - Mean product size and specific crushing energy for material-FM, shape-cylinder, from height-B.

No.	Specimen weight (lb)	Mean product size (inch)	Mean product size (dimensionless)	Standard deviation of product (inch)	Standard deviation of product (dimensionless)	Specimen output energy (ft-lb)	Crushing energy (ft-lb)	Specific crushing energy ($ft\text{-}lb/ft^3$)
1	0.35	0.631	0.421	0.281	0.187	103	117	60440
2	0.32	0.417	0.284	0.157	0.107	93	127	69556
3	0.33	0.648	0.439	0.248	0.168	98	122	65473
4	0.34	0.656	0.442	0.279	0.188	111	109	57791
5	0.33	0.626	0.426	0.276	0.188	96	124	67587
6	0.34	0.572	0.384	0.281	0.189	101	119	62582
7	0.33	0.489	0.332	0.218	0.148	93	127	68682
8	0.34	0.617	0.414	0.291	0.195	103	117	61208
9	0.33	0.429	0.290	0.179	0.121	100	120	64102
10	0.34	0.532	0.357	0.260	0.175	98	122	63968
Average	0.34	0.562	0.379	0.247	0.167	100	120	64139
Composite		0.570	0.382	0.266	0.180			

Table B-23 - Mean product size and specific crushing energy for material-FM, shape-cylinder, from height-1.

No.	Specimen weight (lb)	Mean product size (inch)	Mean product size (dimensionless)	Standard deviation of product (inch)	Standard deviation of product (dimensionless)	Specimen output energy (ft-lb)	Crushing energy (ft-lb)	Specific crushing energy (ft-lb/ft^3)
1	0.32	0.437	0.299	0.184	0.126	129	142	78500
2	0.33	0.417	0.283	0.180	0.122	129	142	76237
3	0.34	0.484	0.325	0.198	0.133	124	147	77195
4	0.34	0.615	0.413	0.288	0.193	139	132	69304
5	0.34	0.493	0.331	0.257	0.173	117	155	81074
6	0.34	0.451	0.303	0.183	0.123	119	152	79747
7	0.34	0.415	0.280	0.189	0.127	119	152	80362
8	0.34	0.458	0.303	0.250	0.168	119	152	80259
9	0.33	0.615	0.416	0.257	0.174	124	147	78860
10	0.34	0.468	0.315	0.267	0.180	124	147	77742
Average	0.34	0.485	0.327	0.225	0.152	124	147	77928
Composite		0.492	0.328	0.239	0.161			

Table B-24 - Mean product size and specific crushing energy for material-FM, shape-cylinder, from height-A.

No.	Specimen weight (lb)	Mean product size (inch)	Mean product size (dimensionless)	Standard deviation of product (inch)	Standard deviation of product (dimensionless)	Specimen output energy (ft-lb)	Crushing energy (ft-lb)	Specific crushing energy (ft-lb/ft^3)
1	0.34	0.426	0.286	0.231	0.155	150	205	107086
2	0.33	0.594	0.402	0.299	0.202	139	215	115410
3	0.34	0.470	0.314	0.250	0.167	139	215	111690
4	0.33	0.446	0.302	0.164	0.111	145	210	112201
5	0.33	0.459	0.311	0.186	0.126	160	194	104841
6	0.33	0.343	0.232	0.169	0.114	156	199	106784
7	0.33	0.347	0.235	0.187	0.126	148	207	111486
8	0.35	0.532	0.354	0.215	0.143	150	205	104298
9	0.33	0.389	0.263	0.224	0.151	136	219	116912
10	0.33	0.343	0.233	0.178	0.121	148	207	112446
Average	0.34	0.435	0.293	0.210	0.142	147	208	110315
Composite		0.445	0.297	0.230	0.155			

APPENDIX C--COMPARISON OF VARIOUS DISTRIBUTION FUNCTION FITS

Table C-1. - Comparison of various distribution function fits - Wausau quartzite, irregular shape

Distribution	Line: Y = A + BX		Correlation coefficient	Coefficient of determination
	Intercept A	Slope B		
WAUSAU QUARTZITE-HEIGHT A, IRREGULAR SHAPE, 30 TESTS				
Negative exponential..	0.000	-0.739	-0.977	0.899
Log Weibull...........	-2.423	1.338	0.968	0.965
Weibull...............	-0.569	1.075	0.983	0.972
Power curve...........	-0.967	0.843	0.966	0.988
Log normal............	-0.034	0.807	0.949	0.928
Normal................	-1.480	1.067	0.994	0.993
WAUSAU QUARTZITE-HEIGHT B, IRREGULAR SHAPE, 30 TESTS				
Negative exponential..	0.000	-0.620	-0.930	0.785
Log Weibull...........	-3.007	1.492	0.979	0.977
Weibull...............	-0.955	1.176	0.975	0.949
Power curve...........	-1.274	0.977	0.991	0.968
Log normal............	-0.317	0.809	0.928	0.900
Normal................	-1.790	1.097	0.997	0.997
WAUSAU QUARTZITE-HEIGHT C, IRREGULAR SHAPE, 30 TESTS				
Negative exponential..	0.000	-0.406	-0.907	0.739
Log Weibull...........	-3.717	1.602	0.984	0.978
Weibull...............	-1.522	1.249	0.969	0.881
Power curve...........	-1.736	1.111	0.983	0.890
Log normal............	-0.715	0.755	0.921	0.838
Normal................	-2.098	1.033	0.997	0.996

Table C-2 - Comparison of various distribution function fits - anorthosite, irregular shape

Distribution	Line: Y = A + BX		Correlation coefficient	Coefficient of determination
	Intercept A	Slope B		
ANORTHOSITE-HEIGHT A, IRREGULAR SHAPE, 30 TESTS				
Negative exponential..	0.000	-0.721	-0.919	0.711
Log Weibull...........	-2.892	1.490	0.983	0.989
Weibull...............	-0.849	1.164	0.970	0.937
Power curve...........	-1.206	0.941	0.992	0.959
Log normal............	-0.222	0.833	0.915	0.880
Normal................	-1.753	1.146	0.996	0.993
ANORTHOSITE-HEIGHT B, IRREGULAR SHAPE, 30 TESTS				
Negative exponential..	0.000	-0.358	-0.856	0.669
Log Weibull...........	-3.798	1.542	0.986	0.982
Weibull...............	-1.693	1.191	0.962	0.818
Power curve...........	-1.878	1.071	0.980	0.819
Log normal............	-0.833	0.702	0.905	0.778
Normal................	-2.128	0.971	0.991	0.979
ANORTHOSITE-HEIGHT C, IRREGULAR SHAPE, 30 TESTS				
Negative exponential..	0.000	-0.233	-0.824	0.594
Log Weibull...........	-4.545	1.630	0.991	0.996
Weibull...............	-2.336	1.233	0.947	0.639
Power curve...........	-2.456	1.152	0.962	0.623
Log normal............	-1.208	0.648	0.885	0.625
Normal................	-2.418	0.913	0.987	0.961

Table C-3 - Comparison of various distribution function fits - Felch marble, irregular shape

Distribution	Line: Y = A + BX Intercept A	Slope B	Correlation coefficient	Coefficient of determination
FELCH MARBLE-HEIGHT A, IRREGULAR SHAPE, 30 TESTS				
Negative exponential..	0.000	-0.768	-0.912	0.652
Log Weibull...........	-3.138	1.633	0.983	0.987
Weibull...............	-0.900	1.276	0.970	0.946
Power curve...........	-1.269	1.038	0.990	0.962
Log normal............	-0.232	0.900	0.915	0.888
Normal................	-1.888	1.240	0.998	0.997
FELCH MARBLE-HEIGHT B, IRREGULAR SHAPE, 30 TESTS				
Negative exponential..	0.000	-0.442	-0.931	0.777
Log Weibull...........	-3.561	1.590	0.980	0.977
Weibull...............	-1.375	1.251	0.973	0.912
Power curve...........	-1.610	1.100	0.987	0.925
Log normal............	-0.618	0.775	0.930	0.866
Normal................	-2.029	1.050	0.998	0.998
FELCH MARBLE-HEIGHT C, IRREGULAR SHAPE, 30 TESTS				
Negative exponential..	0.000	-0.324	-0.852	0.594
Log Weibull...........	-4.565	1.816	0.991	0.990
Weibull...............	-2.097	1.385	0.954	0.739
Power curve...........	-2.261	1.272	0.970	0.721
Log normal............	-1.040	0.758	0.895	0.714
Normal................	-2.453	1.064	0.994	0.984

Table C-4 - Comparison of various distribution function fits - Wausau quartzite, disc shape

Distribution	Line: Y = A + BX		Correlation coefficient	Coefficient of determination
	Intercept A	Slope B		
WAUSAU QUARTZITE-HEIGHT A, DISC SHAPE, 10 TESTS				
Negative exponential..	0.000	-4.175	-0.998	0.982
Log Weibull...........	-0.821	2.750	0.979	0.972
Weibull...............	1.368	0.957	0.992	0.986
Power curve...........	0.131	0.462	0.993	0.974
Log normal............	1.887	1.034	0.978	0.951
Normal................	-0.510	3.058	0.992	0.992
WAUSAU QUARTZITE-HEIGHT 1, DISC SHAPE, 10 TESTS				
Negative exponential..	0.000	-3.018	-0.978	0.886
Log Weibull...........	-1.458	3.170	0.997	0.996
Weibull...............	1.016	1.064	0.974	0.962
Power curve...........	0.060	0.643	0.996	0.993
Log normal............	1.404	1.015	0.944	0.913
Normal................	-0.994	3.125	0.998	0.997
WAUSAU QUARTZITE-HEIGHT B, DISC SHAPE, 10 TESTS				
Negative exponential..	0.000	-2.089	-0.990	0.946
Log Weibull...........	-1.503	2.684	0.995	0.993
Weibull...............	0.595	0.903	0.974	0.954
Power curve...........	-0.098	0.615	0.993	0.981
Log normal............	0.902	0.790	0.951	0.919
Normal................	-0.957	2.411	0.997	0.995
WAUSAU QUARTZITE-HEIGHT 2, DISC SHAPE, 10 TESTS				
Negative exponential..	0.000	-1.728	-0.914	0.795
Log Weibull...........	-1.836	2.539	0.987	0.975
Weibull...............	0.285	0.934	0.942	0.905
Power curve...........	-0.311	0.663	0.987	0.936
Log normal............	0.632	0.789	0.884	0.857
Normal................	-1.194	2.233	0.964	0.955
WAUSAU QUARTZITE-HEIGHT C, DISC SHAPE, 10 TESTS				
Negative exponential..	0.000	-1.327	-0.803	0.427
Log Weibull...........	-2.244	2.483	0.941	0.863
Weibull...............	-0.203	0.885	0.870	0.707
Power curve...........	-0.653	0.670	0.946	0.700
Log normal............	0.209	0.695	0.780	0.665
Normal................	-1.432	2.046	0.885	0.800

Table C-5 - Comparison of various distribution function fits - anorthosite, disc shape

Distribution	Line: Y = A + BX		Correlation coefficient	Coefficient of determination
	Intercept A	Slope B		
ANORTHOSITE-HEIGHT A, DISC SHAPE, 10 TESTS				
Negative exponential..	0.000	-2.942	-0.967	0.858
Log Weibull...........	-1.600	3.337	0.995	0.992
Weibull...............	1.012	1.125	0.977	0.968
Power curve...........	0.074	0.703	0.998	0.996
Log normal............	1.384	1.051	0.943	0.922
Normal................	-1.096	3.230	0.996	0.994
ANORTHOSITE-HEIGHT 1, DISC SHAPE, 10 TESTS				
Negative exponential..	0.000	-1.945	-0.995	0.971
Log Weibull...........	-1.582	2.719	0.989	0.985
Weibull...............	0.564	0.931	0.986	0.973
Power curve...........	-0.092	0.657	0.997	0.992
Log normal............	0.848	0.790	0.968	0.946
Normal................	-0.996	2.370	0.997	0.996
ANORTHOSITE-HEIGHT B, DISC SHAPE, 10 TESTS				
Negative exponential..	0.000	-1.395	-0.986	0.941
Log Weibull...........	-1.931	2.711	0.994	0.992
Weibull...............	0.191	0.914	0.976	0.942
Power curve...........	-0.293	0.708	0.991	0.964
Log normal............	0.464	0.707	0.951	0.912
Normal................	-1.199	2.155	0.996	0.992
ANORTHOSITE-HEIGHT 2, DISC SHAPE, 10 TESTS				
Negative exponential..	0.000	-1.351	-0.859	0.644
Log Weibull...........	-2.202	2.595	0.970	0.929
Weibull...............	-0.040	0.949	0.920	0.816
Power curve...........	-0.513	0.726	0.974	0.831
Log normal............	0.321	0.739	0.847	0.772
Normal................	-1.400	2.115	0.934	0.889
ANORTHOSITE-HEIGHT C, DISC SHAPE, 10 TESTS				
Negative exponential..	0.000	-0.990	-0.772	0.364
Log Weibull...........	-2.549	2.414	0.911	0.769
Weibull...............	-0.562	0.862	0.845	0.569
Power curve...........	-0.909	0.695	0.914	0.547
Log normal............	-0.097	0.625	0.753	0.554
Normal................	-1.574	1.839	0.853	0.719

Table C-6 - Comparison of various distribution function fits - Felch marble, disc shape

Distribution	Line: Y = A + BX		Correlation coefficient	Coefficient of determination
	Intercept A	Slope B		
FELCH MARBLE-HEIGHT A, DISC SHAPE, 10 TESTS				
Negative exponential..	0.000	-3.082	-0.971	0.885
Log Weibull...........	-1.531	3.323	0.992	0.987
Weibull...............	1.082	1.130	0.983	0.980
Power curve...........	0.105	0.695	0.998	0.995
Log normal............	1.463	1.068	0.953	0.939
Normal................	-1.049	3.256	0.997	0.998
FELCH MARBLE-HEIGHT 1, DISC SHAPE, 10 TESTS				
Negative exponential..	0.000	-2.540	-0.977	0.885
Log Weibull...........	-1.674	3.242	0.995	0.995
Weibull...............	0.862	1.092	0.976	0.962
Power curve...........	0.026	0.718	0.996	0.989
Log normal............	1.194	0.981	0.948	0.919
Normal................	-1.117	3.005	0.997	0.996
FELCH MARBLE-HEIGHT B, DISC SHAPE, 10 TESTS				
Negative exponential..	0.000	-1.790	-0.981	0.926
Log Weibull...........	-1.897	3.050	0.995	0.994
Weibull...............	0.492	1.030	0.979	0.961
Power curve...........	-0.123	0.758	0.994	0.985
Log normal............	0.764	0.840	0.953	0.927
Normal................	-1.211	2.561	0.998	0.998
FELCH MARBLE-HEIGHT 2, DISC SHAPE, 10 TESTS				
Negative exponential..	0.000	-1.154	-0.990	0.957
Log Weibull...........	-2.231	2.910	0.992	0.986
Weibull...............	0.060	0.992	0.984	0.963
Power curve...........	-0.354	0.811	0.993	0.980
Log normal............	0.315	0.718	0.966	0.937
Normal................	-1.363	2.161	0.998	0.997
FELCH MARBLE-HEIGHT C, DISC SHAPE, 10 TESTS				
Negative exponential..	0.000	-0.704	-0.994	0.973
Log Weibull...........	-2.549	2.641	0.990	0.981
Weibull...............	-0.463	0.905	0.987	0.960
Power curve...........	-0.719	0.797	0.992	0.971
Log normal............	-0.139	0.584	0.973	0.938
Normal................	-1.499	1.742	0.997	0.995